Research Article

Reconstructing postglacial hydrologic and environmental change in the eastern Kenai Peninsula lowlands using proxy data and mass balance modeling

Ellie Broadman[a]* 🔵, Darrell S. Kaufman[a], R. Scott Anderson[a], Sonya Bogle[a], Matthew Ford[b,c], David Fortin[d], Andrew C. G. Henderson[e], Jack H. Lacey[f], Melanie J. Leng[f,g], Nicholas P. McKay[a] and Samuel E. Muñoz[h]

[a]School of Earth and Sustainability, Northern Arizona University, Flagstaff, Arizona, USA; [b]Department of Ecology, Evolution, and Organismal Biology, Iowa State University, Ames, Iowa, USA; [c]Department of Natural Resource Ecology and Management, Iowa State University, Ames, Iowa, USA; [d]Department of Geography and Planning, University of Saskatchewan, Saskatoon, SK, Canada; [e]School of Geography, Politics & Sociology, Newcastle University, Newcastle upon Tyne, UK; [f]National Environmental Isotope Facility, Isotope Geosciences Facility, British Geological Survey, Keyworth, Nottingham, UK; [g]Centre for Environmental Geochemistry, School of Biosciences, University of Nottingham, Nottingham, UK and [h]Department of Marine and Environmental Science, Marine Science Center, Northeastern University, Nahant, Massachusetts, USA

Abstract

Despite extensive paleoenvironmental research on the postglacial history of the Kenai Peninsula, Alaska, uncertainties remain regarding the region's deglaciation, vegetation development, and past hydroclimate. To elucidate this complex environmental history, we present new proxy datasets from Hidden and Kelly lakes, located in the eastern Kenai lowlands at the foot of the Kenai Mountains, including sedimentological properties (magnetic susceptibility, organic matter, grain size, and biogenic silica), pollen and macrofossils, diatom assemblages, and diatom oxygen isotopes. We use a simple hydrologic and isotope mass balance model to constrain interpretations of the diatom oxygen isotope data. Results reveal that glacier ice retreated from Hidden Lake's headwaters by ca. 13.1 cal ka BP, and that groundwater was an important component of Kelly Lake's hydrologic budget in the Early Holocene. As the forest developed and the climate became wetter in the Middle to Late Holocene, Kelly Lake reached or exceeded its modern level. In the last ca. 75 years, rising temperature caused rapid changes in biogenic silica content and diatom oxygen isotope values. Our findings demonstrate the utility of mass balance modeling to constrain interpretations of paleolimnologic oxygen isotope data, and that groundwater can exert a strong influence on lake water isotopes, potentially confounding interpretations of regional climate.

Keywords: Holocene, Alaska, Kenai Peninsula, lake sediment, diatom oxygen isotopes, groundwater, glacial meltwater, mass balance modeling, pollen, multi-proxy

(Received 28 June 2021; accepted 23 December 2021)

INTRODUCTION

The Late Pleistocene and Holocene paleoenvironmental history of Alaska's Kenai Peninsula (Fig. 1) has long been of interest to geologists and climate scientists (e.g., Cooper, 1942; Karlstrom, 1964) due to the region's multi-phased deglaciation (Reger et al., 2007), spatially and temporally complex transition from tundra to mixed coastal forest (Anderson et al., 2017), and sensitivity to synoptic patterns of ocean and atmospheric variability (Bailey et al., 2019) and modern climate change (Hayward et al., 2017). In recent decades, the development of increasingly sophisticated methods for studying past environments has enhanced our ability to interpret paleoclimate datasets from southern Alaska. For example, developments in our understanding of oxygen isotope systematics and proxy systems have yielded numerous reconstructions of past hydroclimatic change inferred from lake sediment archives in the Kenai Peninsula and surrounding region (e.g., Schiff et al., 2009; Jones et al., 2014, 2019; Broadman et al., 2020).

However, interpreting these datasets remains a challenge because of the many variables that can influence lake water oxygen isotope composition, such as the source of precipitation (e.g., Jones et al., 2014), the balance between precipitation and evaporation (e.g., Anderson et al., 2007), and the hydrological setting of the lake (e.g., Anderson et al., 2013). Because these oxygen isotope based reconstructions must attempt to distinguish among these varied influences, many of these studies feature multi-pronged approaches, such as analyzing data from multiple climate proxies (e.g., Broadman et al., 2020) or evaluating the reproducibility of proxy data from multiple, neighboring lakes (e.g., McKay and Kaufman, 2009; Krawiec et al., 2014). Studies in other regions have demonstrated the utility of interpreting lacustrine oxygen isotope data alongside hydrologic and isotope mass balance modeling to constrain the roles of various

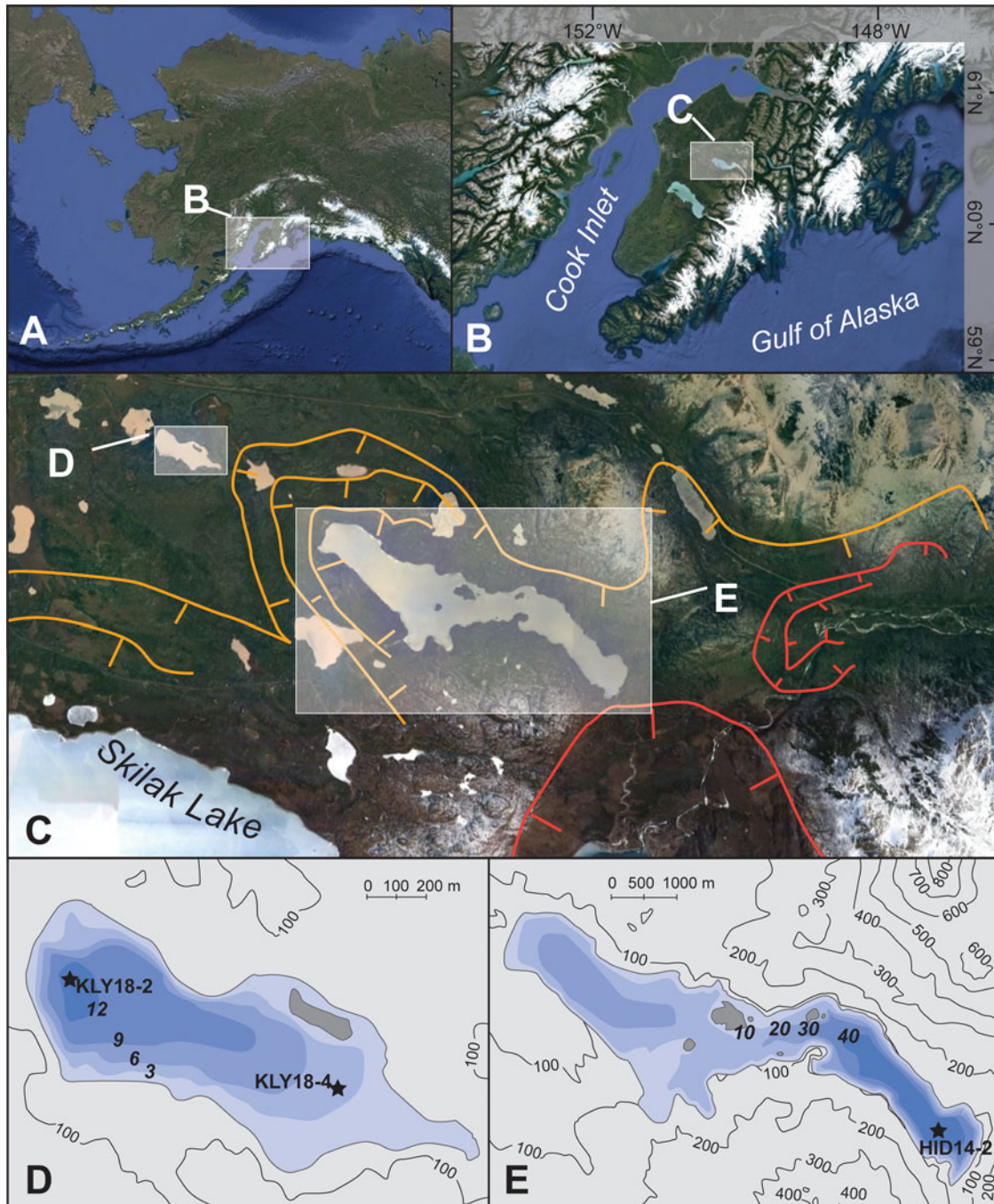**Figure 1.** (**A**) Location of the Kenai Peninsula in Alaska; (**B**) location of the Hidden Lake and Kelly Lake region of the Kenai lowlands; (**C**) glacier margins during the Skilak (orange) and Elmendorf (red) stades of the Naptowne glaciation (Reger et al., 2007), with the location of Kelly (**D**) and Hidden (**E**) Lakes indicated; (**D**) bathymetric map of Kelly Lake; and (**E**) bathymetric map of Hidden Lake; (**D**) and (**E**) show locations of sediment cores discussed in the text. Satellite images from Google Earth.

constituents of a lake's hydrologic budget (e.g., Gibson et al., 2002; Steinman et al., 2010; Lacey and Jones, 2018). These studies, which combine multiple lines of evidence and multiple modes of analysis, are often able to discern the influences of climate and environmental change recorded in proxy datasets, demonstrating the efficacy of these approaches for reconstructing paleoenvironmental conditions.

In southern Alaska, the increasing sophistication and nuance of recently published paleoclimate reconstructions builds on foundational studies that initially demonstrated the interconnectedness of environmental and climate change in the region. For example, Ager (1983) first showed that Late Pleistocene and Holocene climate changes in the Kenai Peninsula were accompanied by pronounced shifts in vegetation communities by analyzing pollen in a sediment sequence from Hidden Lake. The transition between glaciolacustrine sediments and gyttja at this site has also been used to constrain the timing of the retreat of glaciers that emanated from the Kenai Mountains and discharged

into Hidden Lake during the Pleistocene–Holocene transition (Reger et al., 2007). However, these environmental changes are constrained by a radiocarbon chronology consisting of only four ages over ca. 15,000 years, all of which were derived from bulk sediment samples (Ager, 1983). In recent decades, studies have shown that bulk sediment samples incorporate old carbon and can yield ages several millennia older than those from macrofossils collected in the same stratigraphic horizon (Grimm et al., 2009), and technological advances in accelerator mass spectrometry have permitted the analysis of smaller samples than was previously possible (Santos et al., 2007). These advances in our knowledge of radiocarbon, coupled with advances in our ability to analyze and interpret paleoenvironmental data, suggest that re-examining foundational studies (e.g., Ager, 1983) may improve our insights into deglacial and Holocene climate and environmental change on the Kenai Peninsula.

To investigate late glacial and Holocene conditions along the mountain front of the eastern Kenai lowlands, we have developed new multi-proxy paleoclimate datasets from neighboring Hidden and Kelly lakes (Fig. 1C–E). We revisit the foundational pollen record from Hidden Lake (Ager, 1983) and revise the late glacial and Holocene chronology of deglaciation and vegetation change in this region, which we interpret alongside new sedimentological data from this site. We also present Holocene diatom oxygen isotope, diatom assemblage, macrofossil, and sedimentological datasets from Kelly Lake, and use a simple hydrologic and isotope mass balance model to support and quantitatively constrain our interpretations of the diatom oxygen isotope dataset. In particular, we use this modeling approach to investigate the role of groundwater inflow to Kelly Lake during different time periods by providing ranges of plausible values for the other major components of the Kelly Lake hydrological system (precipitation rate, evaporation rate, and the isotope composition of precipitation and groundwater). The simplicity of the modeling framework is useful for constraining the drivers of large hydrologic and isotopic changes at Kelly Lake, because we consider only the most dominant influences on the hydrological budget.

Our findings demonstrate the importance of groundwater in the hydrologic budget at this site, suggesting that climate-driven changes in groundwater inflow can have a profound influence on lake water isotope values. Furthermore, by using varied sedimentological, biological, and geochemical proxy datasets from multiple lakes, coupled with mass balance modeling, we demonstrate the potential of such efforts in creating a multi-faceted reconstruction of paleoenvironmental change.

Study area and regional climate

The Kenai Peninsula is located in south-central Alaska, bordered by Cook Inlet and the Gulf of Alaska (Fig. 1A, B). The Kenai Mountains occupy the southeastern portion of the peninsula and act as a barrier to storms traveling from the North Pacific Ocean, creating a rain shadow effect in the Kenai lowlands to the northwest. Mean annual temperature at the Kenai Moose Pens SNOTEL site was 2.7°C, mean annual rainfall was 47.2 cm, and mean annual snow-water equivalent was 11.4 cm between 1995 and 2019 (National Water and Climate Center, https://www.nrcs.usda.gov/wps/portal/wcc/home/). The majority of precipitation in the Kenai Peninsula occurs from November to March (Fig. 2A), when the Aleutian Low atmospheric pressure cell (AL) strengthens and moves eastward, as opposed to spring and summer months when it weakens and moves westward (Overland et al., 1999).

These seasonal changes in precipitation are accompanied by changes in temperature and the oxygen isotope composition of precipitation (δ_P) (Fig. 2A), where the summer months are warmer, with higher δ_P values. Precipitation-weighted seasonal average δ_P measured in Anchorage are −14.5‰ for summer and −20.7‰ for winter, and −17.7‰ annually (Bailey et al., 2019) (Fig. 2A). Both seasonal and interannual shifts in average storm trajectories associated with AL variability can also influence δ_P (Berkelhammer et al., 2012; Porter et al., 2014). These interannual and longer-term AL fluctuations superimpose an isotope imprint on the average seasonal change in δ_P.

The Kenai Peninsula lowlands are dotted with kettle lakes that formed as the Cordilleran Ice Sheet retreated to both the Kenai Mountains and the Alaska Range following the Naptowne glaciation (Fig. 1C). The retreat of ice from its maximum extent was punctuated by several distinct stades throughout the Late Pleistocene, described by Reger et al. (2007). During the penultimate stade in this progression, the Skilak stade, lakes in the eastern Kenai lowlands located close to the mountains remained heavily influenced or occupied by glaciers. At this time, Kelly Lake (60.516°, −150.380°; 94 m asl) was deglaciated, but received meltwater from the glacier that occupied the Hidden Lake trough (60.485°, −150.267°; 86 m asl), ~4 km to the southeast (Fig. 1C). One event associated with termination of the Skilak stade is retreat of the Hidden Lake lobe, which halted the deposition of rock flour and meltwater in Hidden Lake's catchment. As such, the minimum limiting age for the Skilak stade termination is based on the transition between glaciolacustrine sediment and gyttja in a sediment core previously analyzed from Hidden Lake (Ager, 1983), which is dated at ca. 16.6 ± 0.3 ka cal BP. This date is based on a bulk sediment sample originally analyzed using liquid scintillation (Ager, 1983), and has been recalibrated in this study after Reimer et al. (2020).

The final stade of the Naptowne glaciation, the Elmendorf stade, has been associated with a Late Pleistocene readvance during the Younger Dryas (Reger et al., 2007) and the subsequent retreat of glaciers from the Kenai lowlands by ca. 11 cal ka BP (Fig. 1C). Evidence for this latest stade in the Kenai lowlands is less robust than in the Matanuska and Knik valleys and in the Chugach Mountains, north of the Kenai Peninsula (Reger and Updike, 1983; Reger et al., 1995, 2011; Wiedmer et al., 2010; Kopczynski et al., 2017; Valentino et al., 2021).

Today, glaciers terminate ~25 km southeast of Hidden Lake, and both Kelly and Hidden lakes are surrounded by boreal forest (Fig. 1C). Neither lake has a perennial surface inflow, although each lake has a minor surface outflow. Upwelling subaqueous springs are visible at the shallow eastern edge of Kelly Lake; the groundwater discharge likely comes from one of the two aquifers (surficial and deep) underlying the Kenai lowlands (Eilers et al., 1992).

METHODS

Sediment core recovery and sedimentological analyses

Sediment cores were collected from the depocenters of Hidden Lake (60.47226°, −150.21169°; 40 m water depth; Fig. 1E) and Kelly Lake (60.518770°, −150.39025°; 13 m water depth; Fig. 1D), from a raft in 2014 and 2018, respectively. The Hidden Lake core HD14-2 (252 cm long) and the uppermost 561 cm of the Kelly Lake sediment sequence (KLY18-2A) were collected using a percussion coring system. The stratigraphically
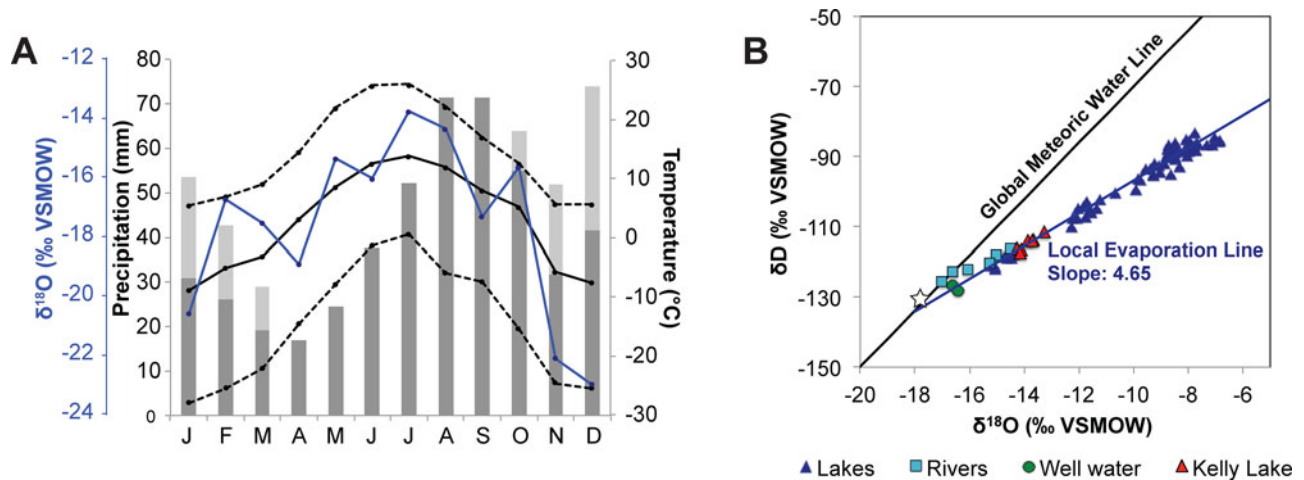
Figure 2. (**A**) Meteorological data from the Kenai Moose Pens SNOTEL station in Soldotna (https://www.nrcs.usda.gov/wps/portal/wcc/home/), showing the average (solid line), high (upper dashed line), and low (lower dashed line) temperatures alongside average monthly precipitation (dark-gray bars) and average monthly snow-water equivalent (SWE; light-gray bars) for 1995–2019 CE. The blue line shows monthly precipitation oxygen isotope values (δ_P) recorded at Tideview Station in Anchorage for 2005–2018 CE (Bailey et al., 2019). (**B**) Water isotope data for lakes, rivers, and groundwater in the Kenai lowlands collected between 2017 and 2018 CE (Broadman et al., 2020), shown with Local Evaporation Line (dark blue) plotted for all lake water samples, and the Global Meteoric Water Line (black). The annual average δ_P, weighted by monthly precipitation amount (shown in A), is indicated by the white star.

lowest sections of the Kelly Lake sediment sequence (KLY18-2B) were collected using a 5-cm-diameter Livingstone piston corer, yielding a total length of 825 cm for composite core KLY18-2. An additional core collected from Kelly Lake, KLY18-4, also has been analyzed by Wrobleski (2021).

Following recovery, cores were transported to the National Lacustrine Core Facility (LacCore) at the University of Minnesota, Minneapolis, where they were split, described, and analyzed for magnetic susceptibility (MS) and reflectance spectroscopy (between 400 and 700 nm) with a Geotek MSCL-XYZ automated core logger at 5 mm spacing. MS was analyzed using a Bartington MS2E surface probe, and reflectance was analyzed using a Konica Minolta spectrometer. The relative absorption-band depth (RABD) between 660 and 670 nm ($RABD_{660;670}$) was calculated using Equation (1):

$$RABD_{660;670} = [(6*R_{590} + 7*R_{730})/13]/R_{min(660;670)} \quad (1)$$

where R_{590} is reflectance at 590 nm, R_{730} is reflectance at 730 nm, and $R_{min(660;670)}$ is the minimum reflectance at either 660 or 670 nm (Rein and Sirocko, 2002). $RABD_{660;670}$ yields an estimate of sedimentary chlorin abundance, the diagenetic product of chlorophyll, which has absorption maxima between 660 and 690 nm (Wolfe et al., 2006). $RABD_{660;670}$ values are proportional to actual chlorin content, with typical values for lake sediments between ∼1 and 2 (Butz et al., 2015).

Additional sedimentological analyses completed for these cores include bulk organic-matter content (OM), grain size distribution, and biogenic silica content (BSi). OM was measured using loss on ignition for every 3–4 cm of HD14-2, and for every 1–2 cm for KLY18-2. Each 1 cm³ (HD14-2) or 2.5 cm³ (KLY18-2) sample was weighed and dried overnight in an oven, then re-weighed and burned at 550°C for 2 hours, and finally weighed again to estimate OM content (Dean, 1974). Grain size analysis was performed on 83 samples at ∼5 cm increments throughout HD14-2. Samples weighing 0.2–0.6 g were treated with 30% H_2O_2 to remove organic matter and 10% Na_2CO_3 to remove biogenic silica, and were subsequently deflocculated in 5%

$Na_6[(PO_3)_6]$. Grain size was measured by laser diffraction using a LS-230 Beckman-Coulter analyzer, with 30 seconds of ultrasonic dispersion completed before each run. Finally, BSi was determined for samples from KLY18-2 using wet-alkaline extraction (10% Na_2CO_3), molybdate-blue reduction, and spectrophotometry (Mortlock and Froelich, 1989). Sampling resolution was every 1 cm for the upper 30 cm, and every 8–9 cm downcore ($n = 130$). A duplicate was analyzed for every 4 or 5 samples ($n = 30$) to determine the reproducibility of the procedure. Duplicates were processed in separate batches, and samples in each batch were selected randomly from all sample depths. Analytical reproducibility of the procedure, as indicated by differences between duplicate samples, averages $1.5 \pm 1.0\%$ (1σ).

Geochronology and proxy time-series correlations

Core chronologies were established using 10 (HD14-2) and 13 (KLY18-2) AMS ^{14}C dates on plant and insect macrofossils (Table 1). For KLY18-2, aquatic plants were avoided due to the presence of a hard water effect. Sediment samples 1 cm thick were sieved at 150 μm, and macrofossils were picked, dried in an oven at 50°C, and identified under a Zeiss light microscope. Macrofossils were prepared and converted to graphite at Northern Arizona University, and ^{14}C content was measured at the Keck-Carbon Cycle AMS facility at UC Irvine. Radiocarbon dates were incorporated into an age model for each sediment sequence using the R package Bacon (v2.5; Blaauw and Christen, 2011), which calibrates ^{14}C years to calendar years using IntCal20 (Reimer et al., 2020).

To supplement the ^{14}C chronology for the Kelly Lake sediment sequence, ^{210}Pb and ^{137}Cs profiles were used to constrain the chronology for the last ca. 170 years of core KLY18-2 (Supplementary Fig. 1; Supplementary Table 1). ^{210}Pb, ^{214}Pb, and ^{137}Cs γ-activities were measured on 20 oven-dried and powdered samples from the upper 50 cm of surface core KLY18-2C using a Canberra Broad Energy Germanium Detector (BEGe; model no. BE3830P-DET) housed at the Marine Science Center

Table 1. Radiocarbon (^{14}C) ages for Hidden Lake core HD14-2 and Kelly Lake core KLY18-2. Depths are given as the midpoint of 1-cm-thick samples below lake floor (blf). Calibrated age is the median of the calibrated age probability density function. Uncertainty is one half of the calibrated two-sigma (2σ) range.

Core ID	Midpoint depth blf (cm)	^{14}C age (yr BP)	Calibrated age (cal yr BP)	Dated material	UCI AMS
HD14-2	42	1590 ± 15	1469 ± 55	wood fragments, seeds	153967
HD14-2	52	1975 ± 50	1903 ± 129	resting eggs, insect chitin, twigs, leaf fragments	147376
HD14-2	71	3150 ± 20	3378 ± 70	resting eggs, insect chitin, twigs, leaf fragments	153966
HD14-2	96	3940 ± 25	4383 ± 76	twigs	147377
HD14-2	128	5675 ± 30	6453 ± 79	twigs	147378
HD14-2	146	6565 ± 35	7469 ± 45	leaf fragments, resting eggs, aquatic plant fragments	147379
HD14-2	155.5	7180 ± 25	7990 ± 39	wood, terrestrial plant fragments	147380
HD14-2	188	8355 ± 30	9373 ± 89	wood	147381
HD14-2	217.5	8770 ± 35	9769 ± 155	aquatic plant fragments, resting eggs	147382*
HD14-2	225	10570 ± 35	12618 ± 52	resting eggs, leaf fragments, insect chitin, twigs	153968
KLY18-2	65.5	595 ± 20	606 ± 29	wood fragments, leaf fragments, insect chitin	209974
KLY18-2	86.5	1160 ± 15	1067 ± 36	aquatic plant branch	208325*
KLY18-2	178.5	1560 ± 15	1458 ± 23	*Betula kenaica* fruits, leaf fragments	208326
KLY18-2	261	2340 ± 20	2349 ± 16	wood, insect chitin	208327
KLY18-2	353.5	2825 ± 20	2924 ± 52	*Betula kenaica* bract, *Betula kenaica* fruit, *Picea* needle, insect chitin, wood fragments	208328
KLY18-2	446	3675 ± 20	4030 ± 63	leaf fragments, wood fragments, *Betula kenaica* fruits, *Betula kenaica* bracts, *Alnus* fruit, bryophyte twig	208329
KLY18-2	544	4345 ± 25	4909 ± 61	*Betula kenaica* fruit, *Alnus* fruit, insect chitin, woody stem, leaf fragments	208330
KLY18-2	565.5	4535 ± 20	5155 ± 68	beetle elytra, *Betula kenaica* fruits, leaf fragments, plant tissue	208331
KLY18-2	647.5	5130 ± 45	5871 ± 53	bark, leaf fragments	208332
KLY18-2	683	6170 ± 30	7068 ± 93	wood fragments, leaf fragments, 2 *Betula kenaica* fruits w/ wing	209975
KLY18-2	736.5	7190 ± 30	7993 ± 46	*Betula kenaica* fruits, *Alnus* fruit, wood fragments, leaf fragments	208333
KLY18-2	779	8320 ± 25	9354 ± 88	2 *Betula kenaica* seeds w/wings, *Betula kenaica* bracht, leaf fragments, wood fragments	209976
KLY18-2	823	9610 ± 40	10940 ± 103	leaf fragments, bryophyte stem, wood fragments, plant stems	208334

*Denotes a sample excluded from the Bacon age models.

of Northeastern University, with a count time of 24 hours. The Constant Rate of Supply (CRS) model (Appleby, 2001) was used to estimate ages and confidence intervals of the samples with excess ^{210}Pb activities above equilibrium with ^{214}Pb.

Because several of the proxy datasets presented in this study are indicators of past productivity (especially chlorin, organic matter [OM], and biogenic silica [BSi] abundances), we calculated the extent to which these time series are correlated. For time series from the same site (either Hidden Lake or Kelly Lake), data were first resampled to average over the intervals of the time series with lower temporal resolution using the software package Analyseries (Paillard et al., 1996), and a correction for autocorrelation was performed (Bretherton et al., 1999). To determine relationships among time series between Hidden and Kelly lakes, the ensemble outputs from the Bacon age models were used to calculate age-uncertain correlations with the R package geoChronR (v.1.0.6; McKay et al., 2021). Proxy data were binned into 500-year intervals prior to correlation. Significance was estimated with an "isospectral" approach, where characteristics of the time series' power spectra are incorporated into significance testing

to assess the impact of autocorrelation and other biases (Ebisuzaki, 1997). To avoid the possibility of test multiplicity when correlating among many ensemble members, a 5% false discovery rate (FDR) correction was applied, which controls for spurious correlations that might arise as an artifact of repeated testing (Benjamini and Hochberg, 1995; Ventura et al., 2004).

Pollen and macrofossils

To correlate the pollen zones identified by Ager (1983) with our dataset from HD14-2, 11 samples from core HD14-2 were analyzed for pollen following standard protocols (Faegri and Iverson, 1989). Using these newly acquired data, the stratigraphic positions of the Ager (1983) pollen zones were located in HD14-2 (Supplementary Table 2), and revised ages were assigned using the output of the Bacon age model. For this study, the pollen data were plotted as percent relative abundance using the R package Rioja (v.0.9-26; Juggins, 2017), and an incremental sum-of-squares cluster analysis (CONISS) was applied (Grimm, 1987) using the R package Vegan (v.2.5-7; Oksanen et al., 2007).

To complement the pollen data from Hidden Lake, 74 samples (1 cm thick; 10 cm increments) from KLY18-2 were analyzed for macrofossils. Limited material in the upper ~50 cm of KLY18-2 excluded these youngest sediments from macrofossil analyses. Samples were deflocculated in 5% $Na_6[(PO_3)_6]$ and then sieved at 125 and 250 µm to isolate macrofossil material. Identifiable terrestrial and aquatic plant macrofossils were counted, and then plotted as concentration per 10 cm^3 using the R package Rioja (v.0.9-26; Juggins, 2017).

Diatom assemblages

Twenty 1-cm-thick samples from KLY18-2 were selected at 25–50 cm increments for diatom species analysis. Samples were treated with 30% H_2O_2 and 70% HNO_3 to remove organic matter, then mounted on slides using Naphrax© medium. A Zeiss light microscope was used to count 300 valves per slide along transects at 1000X, and taxonomic classifications were made according to Foged (1971, 1981), Krammer and Lange-Bertalot (1986–1991), McGlaughlin and Stone (1986), and Mann et al. (2004). Diatom species counts were converted to percent relative abundance and graphed using the R package Rioja (v.0.9-26; Juggins, 2017), and a CONISS analysis was applied to dominant taxa with a relative abundance >5% in at least one sample (Grimm, 1987) to determine zone designations, using the R package Vegan (v.2.5-7; Oksanen et al., 2007). A principal component analysis (PCA) (ter Braak and Prentice, 1988) was completed on the correlation matrix of untransformed percentage data for all dominant taxa. The proportion of planktonic diatoms was calculated as the sum of all planktonic taxa divided by the sum of all planktonic and benthic taxa (excluding facultatively planktonic diatoms) (Wang et al., 2013).

Diatom oxygen isotopes

Samples for diatom oxygen isotope ($\delta^{18}O_{diatom}$) analysis (1 cm thick) were taken from KLY18-2 every ~10 cm down core, and every 1 cm of the upper 25 cm ($n = 107$). Sampling avoided visible tephra layers, as well as basal sediments that contain few diatoms. Samples were purified using a series of chemical digestions, sieving, and heavy liquid separations (Morley et al., 2004). All samples were visually inspected for contamination under a Zeiss light microscope, and 27 samples were inspected further using a Zeiss Supra 40VP variable pressure field emission scanning electron microscope (SEM) (e.g., Supplementary Fig. 2) and energy dispersive X-ray spectroscopy (EDS). $\delta^{18}O_{diatom}$ values were measured using the stepwise fluorination method (Leng and Sloane, 2008) in the stable isotope facility at the British Geological Survey, UK. $\delta^{18}O$ values are reported as per mil (‰) deviations of the isotopic ratio ($^{18}O/^{16}O$) calculated on the VSMOW scale using a within-run laboratory standard calibrated against NBS-28. $\delta^{18}O$ of the standard biogenic silica (BFC) run alongside the sample diatoms was set to + 28.9‰ ($n = 26$) ±0.1‰ (1σ) (Chaplígin et al., 2011). Analytical reproducibility of the sample material was <0.2‰ (1σ).

Hydrologic and isotope mass balance modeling

A simple hydrologic and isotope mass balance model was used (e.g., Gibson et al., 2002; Steinman et al., 2010) to investigate steady state conditions at different intervals during the Holocene (e.g., Lacey and Jones, 2018), to test the sensitivity of the hydrologic budget to changes in multiple inputs during the past, and to calculate the contribution of groundwater to Kelly Lake. Hydrologic (eq. 2) and isotope (eq. 3) mass balance expressions typically used for lake systems at steady state are given as:

$$dV/dT = G_i + P + S_i - G_o - E - S_o = 0 \qquad (2)$$

$$d(V\delta_L)/dT = G_i\delta_{Gi} + P\delta_P + S_i\delta_{Si} - G_o\delta_L - E\delta_E - S_o\delta_L = 0 \qquad (3)$$

where S_i and G_i are the surface and groundwater inflow rates, S_o and G_o are the surface and groundwater outflow rates, P and E are the precipitation and evaporation rates, V is the volume of water in the lake (L), and T is time. In Equation (3), each term in Equation (2) is multiplied by the annually averaged isotope composition of each inflow (i) and outflow (o). Groundwater and surface water outflows (G_o and S_o) are assumed to have the isotope composition of the lake water (δ_L).

$$G_i = [P(\delta_L - \delta_P) + E(\delta_E - \delta_L)]/(\delta_{Gi} - \delta_L) \qquad (4)$$

For the modern period, most terms in Equation (4) can be represented using measured values (Tables 2, 3). For P, the mean annual precipitation rate from 1995–2018 measured at the Kenai Moose Pens SNOTEL station (Fig. 2A) was converted to the volume of on-lake precipitation. The monthly weighted average of annual precipitation oxygen isotopes measured from 2005–2018 at the Tideview Station in Anchorage was used for δ_P (Bailey et al., 2019; Fig. 2A). Measurements of δ_L at Kelly Lake and δ_{Gi} from a well in Sterling, Alaska, were collected in 2017 and 2018 (Broadman et al., 2020; Fig. 2B), and were assumed to be representative of annual average values. The annual average evaporation rate recorded from 1917–2005 at the Western Regional Climate Center in Gateway, Alaska (~130 km northeast of Kelly Lake; https://wrcc.dri.edu/Climate/comp_table_show.php?stype=-pan_evap_avg) is essentially identical (within 0.01 m/year) to that calculated using the Linacre (1992) simplification of the Penman (1948) formula for open water evaporation at Kelly Lake, and this value was used for E.

The isotope composition of evaporated water vapor (δ_E) was estimated using the Craig and Gordon (1965) evaporation model:

$$\delta_E = [(\alpha* \times \delta_L) - (h \times \delta_A) - \varepsilon]/[1 - h + (0.001 \times \varepsilon_K)] \qquad (5)$$

where δ_L is the isotope composition of the lake water. In Equation (5), $\alpha^\star$ is the reciprocal of the equilibrium isotope fractionation factor (α) estimated for $\delta^{18}O$ in Equation (6) using the equation of Horita and Wesolowski (1994), where T_W is the temperature of the lake surface water (in K):

$$ln\alpha = 0.35041(10^6/T_W^3) - 1.6664(10^3/T_W^2) \\ + 6.7123(1/T_W) - 7.685 \times 10^{-3} \qquad (6)$$

The normalized relative humidity (h) used in Equation (5) can be estimated using Equation (7) as the quotient of the saturation vapor pressure of the overlying air (e_{s-a}) and the saturation vapor pressure at the surface water temperature (e_{s-w}) (e.g., Steinman et al., 2010). Both of these can be estimated with Equation (8) using annual average air temperature and surface lake water temperature, respectively. Annual average surface

Table 2. Climate and hydrologic variables used as inputs for the Kelly Lake hydrologic and isotope mass balance modeling for each time period discussed in the text. Values are for annual averages.

Time period	Variable	Value	Source
Modern	Air temperature	3.0°C	Kenai Moose Pens SNOTEL site*
	Water temperature	9.5°C	Discovery Pond (see supplementary data)
	Relative humidity	89%	NCEP/NCAR Reanalysis (Kalnay et al., 1996)
	Kelly Lake surface area	0.59 km²	Kenai National Wildlife Refuge data**
	Kelly Lake water δ^{18}O	−13.9‰ VSMOW	measured (Broadman et al., 2020)
Middle–late Holocene (7–0 cal ka BP)	Air temperature	1.0°C	HadCM3 4 ka snapshot simulation
	Water temperature	7.5°C	estimated assuming the same offset between air and lake temperature in the modern measurements
	Relative humidity	89%	HadCM3 4 ka snapshot simulation
	Kelly Lake surface area	0.60 km²	estimated in Google Earth based on maximum paleoshorelines visible in satellite imagery
	Kelly Lake water δ^{18}O	−11.0‰ VSMOW	estimated from δ^{18}O$_{diatom}$ (Crespin et al., 2010)
Early Holocene (10–9 cal ka BP)	Air temperature	0.5°C	HadCM3 9 ka snapshot simulation
	Water temperature	7.0°C	estimated assuming the same offset between air and lake temperature in the modern measurements
	Relative humidity	92%	HadCM3 9 ka snapshot simulation
	Kelly Lake surface area	0.45 km²	estimated in Google Earth based on location of KLY18-4 and an assumed lake level lowstand
	Kelly Lake water δ^{18}O	−15.7‰ VSMOW	estimated from δ^{18}O$_{diatom}$ (Crespin et al., 2010)

*Data for 1995–2018 from the National Water and Climate Center: https://www.nrcs.usda.gov/wps/portal/wcc/home/
**Data from the US Fish and Wildlife Service: https://www.fws.gov/refuge/Kenai/map.html

relative humidity (*RH*) for 1995–2018 was taken from the Kelly Lake grid cell of the NCEP/NCAR Reanalysis (Kalnay et al., 1996).

$$h = RH \times (e_{s-a}/e_{s-w}) \qquad (7)$$

$$e_{s-a \& s-w} = 6.108 \times e^{[(17.27 \times T)/(T+237.7)]} \qquad (8)$$

In lieu of year-round measurements of surface water temperature at Kelly Lake, we used the annual average surface water temperature measured from 2005–2007 at nearby Discovery Pond (∼40 km to the northwest) in Equation (8) (Table 2; Supplementary Data).

The isotope composition of atmospheric moisture (δ_A) used in Equation (5) is assumed to be in equilibrium with precipitation in Equation (9). The equilibrium isotope separation factor (ε^*) is the difference between the isotope composition of precipitation and atmospheric moisture (Gibson et al., 2002; eq. 10), known to be a function of temperature (Gonfiantini, 1986; eq. 6). The total isotope separation factor (ε; eq. 11) also comprises a kinetic component (ε_K; Gibson et al., 2002), which can be constrained for oxygen isotope fractionation (Gonfiantini, 1986; eq. 12).

$$\delta_A = \delta_P - \varepsilon^* \qquad (9)$$

$$\varepsilon^* = 1000 \times (1 - \alpha^*) \qquad (10)$$

$$\varepsilon = \varepsilon^* + \varepsilon_K \qquad (11)$$

$$\varepsilon_K = 14.2 \times (1 - h) \qquad (12)$$

To use the Krabbenhoft et al. (1990) model (eq. 4) to investigate past environmental conditions, variables must be inferred from climate model output or derived empirically. Deriving δ_E (eq. 5) requires estimates for *RH,* air temperature, and water temperature; for these, and for estimates of *P* and *E*, we used the original (not downscaled) output of "snapshot" simulations performed using the coupled ocean-atmosphere circulation model HadCM3 (Singarayer and Valdes, 2010) (Tables 2, 3). Estimates were taken from snapshots for 9 ka (to investigate the Early Holocene) and 4 ka (to investigate the Middle to Late Holocene). Although approximate, these simulations provide appropriate past annual average baseline conditions that we used to assess hydrologic and isotope mass balance at Kelly Lake.

As might be expected, the mean values of variables from the climate simulation are somewhat different from the observed values for these variables near Kelly Lake (Supplementary Table 3). Simulated surface air temperature is ∼2–3°C lower than observed at Kenai airport (air temperature; https://www.ncdc.noaa.gov/cdo-web/datasets), simulated precipitation is 0.05 m/year higher than observed at the Kenai Moose Pens SNOTEL station, and simulated evaporation is 0.09 m/year lower than observed at the Western Regional Climate Center station in Gateway. This might be because of relatively low-resolution parameterization and lack of downscaling, or because the simulations are not fully transient (Singarayer and Valdes, 2010), both of which might result in simulated conditions that fail to fully account for feedbacks of slow-responding components of the climate system. As such, for variables inferred from the HadCM3 simulations, we performed a bias adjustment by calculating the difference between observed recent climate data and the 0 ka

Table 3. Measurements and fluxes for hydrologic and isotopic inflows (precipitation, groundwater) and outflows (evaporation) used in the Kelly Lake modeling and sensitivity testing for each time period.

Time period	Variable	Flow rate (m/year)	Volume (km³/year)	δ¹⁸O (‰ VSMOW)	Source
Modern	Precipitation	0.59	3.5E-04	−17.7	Flow rate: Kenai Moose Pens SNOTEL site* $\underline{\delta^{18}O}$: measured (Broadman et al., 2020)
	Evaporation	0.44	2.6E-04	−20.2	Flow rate: Matanuska AES pan evaporation** $\underline{\delta^{18}O}$: derived (see text)
	Groundwater	—	1.2E-04	−16.5	Flow rate: estimated in this study $\underline{\delta^{18}O}$: measured (Broadman et al., 2020)
Middle–late Holocene (7–0 cal ka BP)	Precipitation	0.61	range of possibilities depending on scenario	−14.7, −17.7, −20.7	Flow rate: HadCM3 4 ka snapshot simulation $\underline{\delta^{18}O}$: scenarios for δ_P higher, similar to, and lower than today
	Evaporation	0.45	range of possibilities depending on scenario	−17.0, −30.4, −35.8	Flow rate: HadCM3 4 ka snapshot simulation $\underline{\delta^{18}O}$: derived (see text)
	Groundwater	—	range of possibilities depending on scenario	ranges from −13.2 to −22.2 depending on scenario (assuming δ_{Gi} differs from δ_P by up to 1.5‰)	Flow rate: estimated in this study $\underline{\delta^{18}O}$: range of possibilities inferred from δ_P
Early Holocene (10–9 cal ka BP)	Precipitation	0.50	range of possibilities depending on scenario	−17.7, −20.7	Flow rate: HadCM3 9 ka snapshot simulation $\underline{\delta^{18}O}$: scenarios for δ_P higher, similar to, and lower than today
	Evaporation	0.32	range of possibilities depending on scenario	−30.4, −35.8	Flow rate: HadCM3 9 ka snapshot simulation $\underline{\delta^{18}O}$: derived (see text)
	Groundwater	—	range of possibilities depending on scenario	ranges from −16.2 to −22.2 depending on scenario (assuming δ_{Gi} differs from δ_P by up to 1.5‰)	Flow rate: estimated in this study $\underline{\delta^{18}O}$: range of possibilities inferred from δ_P

*Data for 1995–2018 from the National Water and Climate Center: https://www.wcc.nrcs.usda.gov/index.html
**Data from the Western Regional Climate Center: https://www.nrcs.usda.gov/wps/portal/wcc/home/

HadCM3 simulation, and then applying this difference to the 9 ka and 4 ka values for each variable (Supplementary Table 3). This bias adjustment allows for a direct comparison between modern conditions at Kelly Lake, and the simulated difference between modern and past conditions. The offset between the surface air temperature and the surface water temperature was assumed to be equal to that recorded in the modern period at Discovery Pond (Table 2).

Estimates for *P* and *E* in Equation (4) require values both for precipitation and evaporation rates, and for lake surface area (Table 2). Uncertainties in the precipitation and evaporation rates were incorporated into sensitivity testing by modeling scenarios where *P* and *E* might be up to 25% higher or lower compared to the HadCM3-inferred values. Current and estimated maximum lake surface areas were measured from Google Earth satellite imagery taken in 2019. An estimate for the minimum lake surface area was based on bathymetry and evidence for continuous postglacial sedimentation at the shallow water core site, KLY18-4 (Wrobleski, 2021; Supplementary Fig. 3).

The approximate isotope composition of past lake water (δ_L) in Equation (4) was inferred from sedimentary $\delta^{18}O_{diatom}$ values (Table 2). These estimates capture the magnitude of past changes, but the absolute value of past δ_L depends on the oxygen isotope fractionation factor between sedimentary diatom silica and lake water. There is consensus that this temperature-dependent equilibrium fractionation factor between cultured or living diatoms and lake water is approximately −0.2‰/°C (Brandriss et al., 1998; Moschen et al., 2005; Crespin et al., 2010; Dodd and Sharp, 2010). However, calibration studies based on sedimentary diatoms have yielded fractionation factors as large as −0.49‰/°C (Juillet-Leclerc and Labeyrie, 1987; Shemesh et al., 1992), and a growing body of evidence suggests rapid geochemical alteration may overprint the $\delta^{18}O$ of diatom silica in the decades following deposition (Dodd et al., 2017; Menicucci et al., 2017; Tyler et al., 2017). There is no clear solution to account for this possible diagenetic alteration in paleoenvironmental reconstructions, but we acknowledge that it adds uncertainty to reconstructing δ_L based on sedimentary $\delta^{18}O_{diatom}$. However, the lack of a consistent trend over the past several centuries among the $\delta^{18}O_{diatom}$ values in datasets from this region (e.g., Schiff et al., 2009; Bailey et al., 2018; Broadman et al., 2020; this study) indicates that these diagenetic effects are unlikely to systematically affect paleoenvironmental interpretations based on sedimentary $\delta^{18}O_{diatom}$ data.

Inferring δ_L from $\delta^{18}O_{diatom}$ also requires consideration of diatom ecology and diatom oxygen isotope systematics. Oxygen isotope fractionation between diatom silica and lake water occurs not only while a diatom is alive, but also while it sinks through the water column and settles on the lake floor (Dodd and Sharp, 2010; Dodd et al., 2012; Tyler et al., 2017). Therefore, while a diatom might dwell in the water column or near the water's surface during its life, the isotope signature recorded in a sedimentary diatom frustule will be at least partially overwritten by fractionation occurring at the lake floor. As such, we used 4°C as an estimate of average annual bottom water temperature (Vallentyne, 1957) to examine the modern (2018) relationship between δ_L and $\delta^{18}O_{diatom}$ in Kelly Lake surface sediments. We found that the fractionation factor of −1.16‰/°C calculated by Crespin et al. (2010) (eq. 13), which can be rearranged to calculate δ_L (eq. 14), best captures the relationship between temperature, δ_L, and $\delta^{18}O_{diatom}$

at our site:

$$T = 245.3 - 6.25(\delta^{18}O_{diatom} - \delta_L) \qquad (13)$$

$$\delta_L = [[(T - 245.3)/-6.25] - \delta^{18}O_{diatom}] \times -1 \qquad (14)$$

where *T* is in °C, and $\delta^{18}O$ values are in ‰ VSMOW. For the modern calculation, the average of the three youngest Kelly Lake $\delta^{18}O_{diatom}$ values was used (from the uppermost 3 cm; mean = +24.6‰) to account for the probable effects of bioturbation and sediment mixing on the unconsolidated uppermost lake sediments. Using this modern $\delta^{18}O_{diatom}$ value and a temperature of 4°C, Equation (14) yields a δ_L value of −14.0‰, which is analytically indistinguishable from the measured average value of −13.9‰ for Kelly Lake water (Broadman et al., 2020; Fig. 2B).

Equation (4) also requires an estimate of δ_P, which is difficult to constrain with certainty for past periods, because few Holocene isotope-enabled model simulations exist, especially for the Early Holocene. Therefore, we tested scenarios where δ_P values are much higher compared with today (similar to summer precipitation; −14.7‰), much lower compared with today (similar to winter precipitation −20.7‰), and similar to the modern annual average (−17.7‰). These values are in line with the magnitude of δ_P fluctuations inferred from other nearby paleo oxygen isotope datasets (Jones et al., 2014, 2019; Bailey et al., 2018; Broadman et al., 2020) (Table 3). Δ_{Gi} is heavily influenced by δ_P, and therefore was assumed to be within 1.5% of δ_P in all scenarios (Table 3). These scenarios were used to determine the components of the lake's hydrologic budget that most likely caused inferred changes in δ_L, as reflected by sedimentary $\delta^{18}O_{diatom}$, during different intervals of the Holocene. Tests were performed for three time periods: (1) modern, (2) Early Holocene (using inputs from the 9 ka HadCM3 snapshot), and (3) Middle to Late Holocene (using inputs from the 4 ka HadCM3 snapshot).

When determining model inputs for δ_P and δ_{Gi} in Equation (4), necessary reasonable assumptions were made to ensure logical results (i.e., a positive value for G_i). To use this mass balance model (eq. 4), the values for δ_P, δ_E, and δ_{Gi} must all be lower than δ_L (Krabbenhoft et al., 1990). δ_E is empirically derived (described above), and is necessarily lower than δ_L (Craig and Gordon, 1965). It is also reasonable to assume that δ_L is always higher than the annual averages of both δ_P and δ_{Gi} (e.g., Fig. 2B) due to the effects of evaporative isotope enrichment, a phenomenon that does not significantly affect either δ_P or δ_{Gi}. The assumption that δ_L is always higher than δ_{Gi} is critical for this simplified model, because *Gi* asymptotes as δ_L approaches δ_{Gi}. Consequently, we do not simulate conditions where $\delta_L - \delta_{Gi} < 0.5$, and we did not model scenarios where δ_P or δ_{Gi} values violated this or any other aforementioned assumptions of the mass balance model equation.

RESULTS

Sediment properties

Basal sediments of the Hidden Lake core HD14-2 are composed of interbedded, gray, inorganic clay and silt, assumed to have been deposited while glaciers occupied the catchment. Postglacial sediments (above 228.2 cm) from HD14-2 are composed primarily of gyttja, which is interbedded with gray silt

and clay for the stratigraphically lowest ~60 cm (Fig. 3). The sediment sequence contains 15 visible tephra beds (≥1 mm thick) that correspond to peaks in MS (Fig. 3; Supplementary Table 4). Above 228.2 cm, organic matter content (as measured by LOI) fluctuates between 1.5 and 21.0% (mean = 10.0%), and inferred chlorin content (as measured by $RABD_{660;670}$) fluctuates between 1.00 and 1.18 (mean = 1.07). Median grain size (d50) ranges from 5–24 μm, and the coarsest grain-size fraction (d90) ranges from 32–175 μm (Fig. 3).

Kelly Lake sediments are predominantly composed of gyttja, with 27 visible tephra beds (≥1 mm thick) that correspond to peaks in MS (Fig. 4; Supplementary Table 4). The basal ~60 cm of KLY18-2 is carbonate-rich mud interbedded with organic-rich clastic layers (Fig. 4). OM content ranges from 7–92% (mean = 33%), and inferred chlorin content ranges from 0.87–2.55 (mean = 1.33). BSi ranges from 1.0–34.6% (mean = 24.6%), with the lowest values in the basal carbonate mud. Correlations among indicators of past productivity (chlorin, organic matter, and BSi abundances) are shown for datasets within the same lake (Supplementary Fig. 4), and for datasets between different lakes (Supplementary Fig. 5) as histograms for the age-uncertain correlations.

Geochronology

The oldest ^{14}C age from Hidden Lake core HD14-2 is 12,618 ± 97 cal yr BP at 216.7 cm, 11.5 cm above the transition from glaciolacustrine mud to organic-rich sediment (Table 1). The extrapolated age for this transition is 13,089 ± 671 cal yr BP (Fig. 5). The average 95% confidence interval of the Bacon age model, evaluated every 1 cm back to 13,824 ± 955 cal yr BP, is ± 756 years (min = 4; max = 1909 years). One ^{14}C age was excluded from the age model (UCIAMS 147382) because it deviates from the roughly linear downcore trend from the other ^{14}C ages. Average sediment accumulation rate for the postglacial sediment (above 228.2 cm) is 0.17 mm/year. The Hayes tephra, identified at 79.2 cm in Hidden Lake and 473.0 cm in Kelly Lake based on preliminary geochemical analyses (B. Jensen, personal communication, 2020), is dated at 3837 ± 302 cal yr BP and 4234 ± 180 cal yr BP, respectively (Supplementary Table 4). These age ranges are consistent with previous estimates for the multiple deposits associated with Hayes eruptions at this time (Wallace et al., 2014; Davies et al., 2016).

The oldest ^{14}C age from Kelly Lake core KLY18-2 is 10,940 ± 200 cal yr BP at 823 cm, which is at the base of the core. The average 95% confidence interval for the age model is ± 200 years (min = 1; max = 683 years). One ^{14}C age from an aquatic plant stem (UCIAMS 208325) was excluded from the age model; the sample was analyzed prior to realizing the influence of the hard water effect (Philippsen, 2013) on aquatic macrofossil samples from Kelly Lake. Sedimentation rate increases from ~0.4 mm/year to 1.0 mm/year, starting at ca. 6500 cal yr BP. The ^{210}Pb activities exhibit a gradual decline over the upper 36 cm of core KLY18-2C towards an equilibrium of ~11.7 Bq/kg (Supplementary Fig. 1; Supplementary Table 1). The peak in ^{137}Cs activity at 16.5 cm (Supplementary Fig. 1) was used as a reference level to constrain the ^{210}Pb model (Appleby, 2001).

Pollen

Using the pollen data from core HD14-2, we detected the stratigraphic positions of the pollen zone transitions identified by Ager (1983) (Supplementary Table 2) in the new sediment sequence and determined ages for these zones according to the Bacon age model (Fig. 6). Ager (1983) described five major pollen zones, listed below, with the original stratigraphic depths from Ager (1983) and our updated ages from HD14-2.

Zone 1 (13.6–12.9 cal ka BP; 290–260 cm)
Zone 1, the "herb zone," is characterized by a high relative abundance of Cyperaceae (sedge) pollen, as well as the presence of Poaceae (grasses) and *Artemisia* (mugwort, wormwood, sagebrush). *Salix* (willow) is present (~5–10% abundance), probably as a dwarf shrub (Ager, 1983), as has been inferred for other sites in the Kenai lowlands (e.g., Anderson et al., 2006, 2019). Arboreal taxa are absent from this zone, suggesting a landscape dominated by herbaceous taxa.

Zone 2 (12.9–11.0 cal ka BP; 260–205 cm)
Zone 2, the "*Betula* zone," is dominated by *Betula* (birch) pollen, interpreted by Ager (1983) to reflect a dwarf-birch shrub tundra. *Salix* and tundra taxa that are dominant in Zone 1 remain present.

Zone 3 (11.0–9.3 cal ka BP; 205–190 cm)
Zone 3, the "*Populus* and *Salix* zone," is characterized by a decrease in the abundance of *Betula* and an increase in the abundance of *Populus* (cottonwood) and *Salix* pollen. Herbaceous taxa remain present. The first occurrence of *Alnus* (alder) is recorded this zone. These changes indicate a transition from dwarf-birch tundra to a mixture of scrub forest and shrub tundra (Ager, 1983).

Zone 4 (9.3–8.6 cal ka BP; 190–170 cm)
Zone 4, the "*Alnus* zone," is characterized by high *Alnus* pollen values and declines in the abundance of all other taxa, indicating the development of an alder woodland. *Picea* (spruce) makes its first appearance at the end of this zone.

Zone 5 (8.6 cal ka BP–present; 170–0 cm)
Zone 5, the "*Picea*, *Alnus*, and *Betula* zone," is characterized by the increased relative abundance of *Picea* pollen and the continued presence of *Betula* and *Alnus*. Most other previously documented taxa remain present, but in low abundances (<5%). These pollen data indicate the transition from an alder woodland to a spruce, birch, and alder forest (Ager, 1983). *Tsuga mertensiana* (mountain hemlock) pollen appears in the upper 80 cm, indicating arrival of the species in the region at this point. Although we do not have a clear tie point to relate the arrival of *T. mertensiana* to our new age model, if we assume a linear sediment accumulation rate between the sediment surface and the first dated pollen zone transition reported by Ager (1983), this event can be crudely estimated at ca. 4 cal ka BP, which is ca. 1000–2000 years earlier than suggested for the Kenai Peninsula by Anderson et al. (2017).

Macrofossils

The Kelly Lake terrestrial macrofossil data reveal shifts in the vegetation communities of the catchment from ca. 10,300–500 cal yr BP (Fig. 7), which closely reflects the vegetation transitions indicated by the Hidden Lake pollen data. *Betula* bracts and/or fruits are present throughout the nearly 11,000-year sediment sequence, whereas *Alnus* bracts and fruits and *Picea* needles first appear at ca. 8155 cal yr BP (Fig. 7). Bryophytes (mosses) are present continually throughout the sediment sequence. In addition, bryozoan
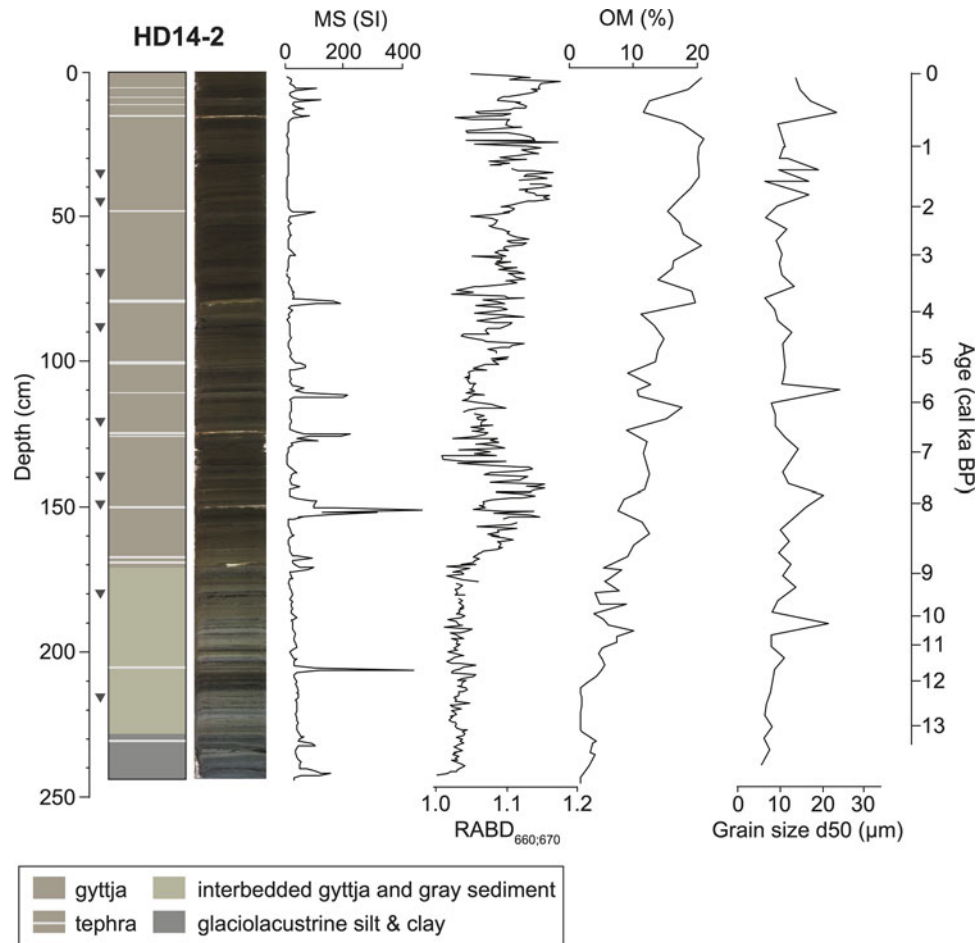
Figure 3. Stratigraphy of Hidden Lake core HD14-2 with magnetic susceptibility (MS), inferred chlorin content (RABD$_{660;670}$), organic matter (OM), and the 50th percentile of clastic grain size (d50). Age scale is based on the age model shown in Figure 5. Gray triangles show calibrated ^{14}C ages listed in Table 1.

statocysts (zooids) are present intermittently, but are concentrated in the sediments prior to ca. 8000 cal yr BP and again following ca. 5000 cal yr BP. *Chara* oospores, which are most prevalent prior to ca. 5500 cal yr BP, persist until ~ca. 900 cal yr BP.

Diatom assemblages

The diatom assemblages from Kelly Lake are diverse, comprising 148 taxa in total, from which 12 species were classified as dominant (those with a relative abundance of >5% in at least one sample) (Fig. 8). Diatoms were too few to count in the basal carbonate-rich mud, and the diatom assemblage data therefore extend back to ca. 9.2 cal ka BP. Dominant species were grouped into one of three habitat types, as specified by Spaulding et al. (2020): (1) planktonic diatoms, which are non-motile and occupy the water column; (2) facultatively planktonic diatoms, which may be motile, often dwelling in the lake's benthos, but can live in the water column when it is ecologically advantageous; and (3) benthic diatoms, which can be motile, or live attached to substrates on the lake floor or in shallow sediments. Dominant genera at Kelly Lake include planktonic (*Aulacoseira*, *Discostella*), facultatively planktonic (*Staurosira*, *Staurosirella*), and benthic (*Pseudostaurosira*, *Staurosirella*) diatoms. Based on the CONISS dendrogram, changes in the relative abundances of these taxa were divided into two main zones (Fig. 8).

Zone 1 (9.2–5.0 cal ka BP; 772–543 cm)

Zone 1 is characterized by high abundances of facultatively planktonic taxa, especially *Staurosira construens* var. *venter*, and including *Pseudostaurosira brevistriata*, *Staurosira construens*, *Staurosirella pinnata*, and *Ulnaria acus*. Benthic taxa are present in relatively low abundances, including *Pseudostaurosira parasitica*, *P. pseudoconstruens*, *Staurosirella martyi*, and, in the most recent part of this zone, *Ulnaria acus*. Planktonic taxa are absent at first, although *Stephanodiscus niagarae* and *Discostella stelligera* appear in low abundances near the end of this zone, followed by *Aulacoseira subarctica*.

Zone 2 (5.0 cal ka BP–present; 543–0 cm)

Zone 2 features the expansion of planktonic taxa, most notably *Aulacoseira subarctica*. *Aulacoseira ambigua* makes its first appearance in this zone, though abundances remain low. *Stephanodiscus niagarae* and *Discostella stelligera* also remain present throughout this zone, with their abundances fluctuating over time. All facultatively planktonic and benthic taxa remain present throughout this zone. Facultatively planktonic diatoms, especially *Staurosira construens* var. *venter* and *S. construens*, are among the more prevalent taxa, whereas benthic species remain present in low abundances throughout. Toward the end of this zone, the abundances of *Pseudostaurosira parasitica* and *P. pseudoconstruens* increase.
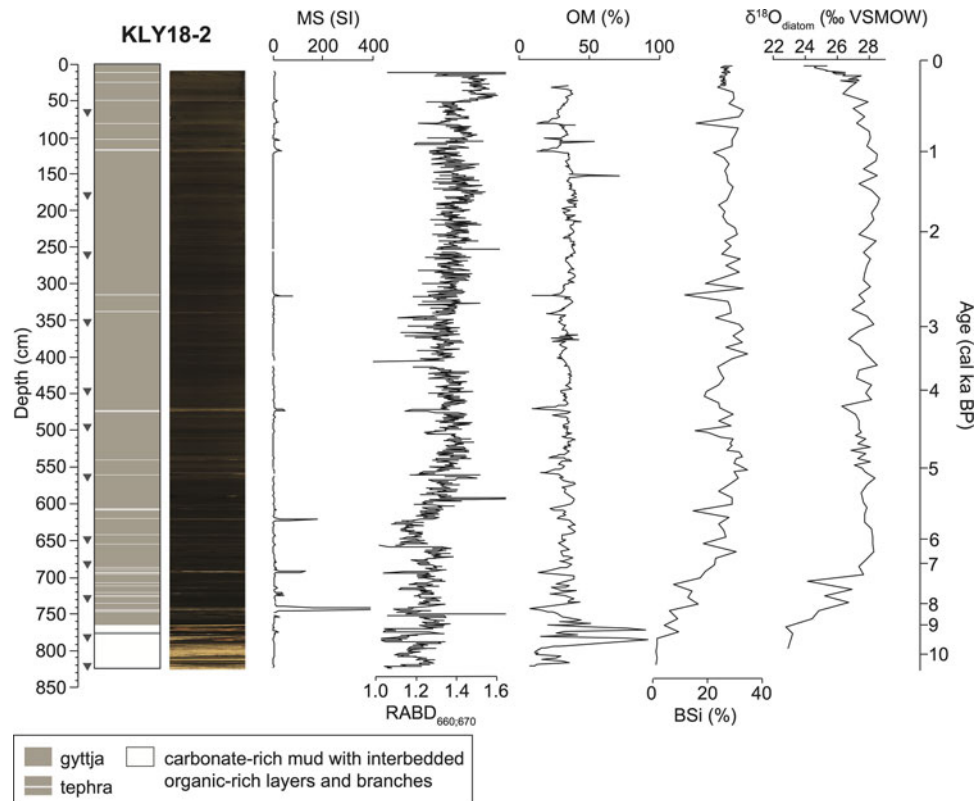
Figure 4. Stratigraphy of Kelly Lake core KLY18-2 with magnetic susceptibility (MS), inferred chlorin content (RABD$_{660;670}$), organic matter (OM), biogenic silica (BSi), and diatom oxygen isotopes ($\delta^{18}O_{diatom}$). Age scale is based on the age model shown in Figure 5. Gray triangles show calibrated ^{14}C ages listed in Table 1.

The first two principal components (PCs) of the stratigraphic diatom assemblage data account for 65% of the overall variance in the record ($\lambda_1 = 0.52$; $\lambda_2 = 0.13$). PC1 largely tracks changes in *Aulacoseira subarctica* (λ_1), whereas PC2 is controlled by variations in numerous other species, most notably by the opposing relation of *Discostella stelligera* and *Pseudostaurosira pseudoconstruens* versus *Staurosira construens* and *S. construens* var. *venter* (Fig. 8; Supplementary Fig. 6).

Diatom oxygen isotopes

The Kelly Lake $\delta^{18}O_{diatom}$ data, which cover the last ca. 9.7 cal ka BP (Fig. 4), show a range of 5.9‰ (+22.7 to + 28.6‰, $n = 107$), with a mean of + 27.0‰. The mean is + 24.5‰ ($n = 9$) prior to 7.3 cal ka BP, then shifts to + 27.6‰ ($n = 83$) between 7.3 cal ka BP and ca. 1960 CE, followed by a decrease to + 25.4‰ ($n = 15$) over the past ca. 60 years (Fig. 4). SEM images indicate that contamination by clay minerals and tephras is insignificant (e.g., Supplementary Fig. 2). EDS data reveal that the percent of Al$_2$O$_3$, commonly used as an indicator of siliceous clay contamination in purified biogenic silica (Brewer et al., 2008), is <1% in all samples. Because sedimentary diatom frustules may contain up to 1% Al$_2$O$_3$ incorporated into the silica matrix (Koning et al., 2007), this result further indicates that samples analyzed for $\delta^{18}O_{diatom}$ comprise pure biogenic silica.

Hydrologic and isotope mass balance modeling

Hydrologic and isotope mass balance calculations (Krabbenhoft et al., 1990) for the modern period suggest that groundwater inflow amounts to 1.2×10^{-4} km^3/year, compared to 3.5×10^{-4} km^3/year for on-lake precipitation and 2.6×10^{-4} km^3/year for lake surface evaporation (Table 3). Using a fractionation factor of $-0.16‰/°C$ between lake water (4°C) and diatom silica (Crespin et al., 2010), δ_L for Kelly Lake in the Early Holocene (ca. 9.8–9.0 cal ka BP) was estimated to be $-15.7‰$, and $-11.0‰$ for much of the Middle and Late Holocene (ca. 7.0–0 cal ka BP) (Table 2). For these calculations (eq. 14), $\delta^{18}O_{diatom}$ values were averaged over the time intervals of interest ($n = 3$, average = +22.9‰ for the Early Holocene; $n = 80$, average = +27.6‰ for the Middle to Late Holocene).

Output of the sensitivity tests reveals the quantity of *Gi* needed to produce our inferred (for the past) or measured (for the present) δ_L values in the Middle to Late Holocene (Fig. 9A–C), the Early Holocene (Fig. 9D, E), and the modern period (Fig. 9F, G). For the modern period, this output demonstrates the sensitivity of the results to the variables of interest. For past climate intervals, results reveal a range of possibilities for *Gi*, depending on input values for δ_P, and consequently δ_{Gi}. Scenarios that yielded negative *Gi* values (indicating a net seepage from the lake to the groundwater) were considered unrealistic because the lake is known to be spring fed, therefore these were excluded from the presented results. An additional scenario is presented for the Middle to Late Holocene, where δ_P is elevated compared to that of modern annually averaged precipitation (Fig. 9C). This δ_P scenario violates the previously discussed model assumptions for both the Early Holocene and the modern time period, because inferred δ_L values at these times are lower than this higher δ_P value; this illustrates how the modeling exercise, combined with the $\delta^{18}O_{diatom}$ data, provides a reasonable constraint on past δ_P.

DISCUSSION

Controls on proxy records at Hidden and Kelly lakes

The datasets presented in this study encompass a broad array of paleoclimate proxies (chlorin, organic matter, grain size, biogenic silica, pollen, macrofossils, diatoms, and diatom oxygen isotopes), each of which reflects different aspects of past environmental conditions. By interpreting these datasets together, in two neighboring lakes with closely related environmental histories, we are able to reconstruct multiple features of regional paleoenvironmental change.

Indicators of past productivity

Chlorin is the diagenetic product of chlorophyll (Rein and Sirocko, 2002), and therefore reflects changes in both terrestrial and aquatic photosynthetic organisms in the lakes and their catchments. The correlation between chlorin content at Hidden and Kelly lakes throughout the Holocene (median $r = 0.64$; $p < 0.05$ for 100% of ensembles; Figs. 3, 4; Supplementary Fig. 5) demonstrates that these data reflect processes that are not catchment specific and represent extra-local landscape patterns.

Chlorin abundance tends to be strongly related to OM fluctuations, which typically represent combined autochthonous and allochthonous OM tied to catchment-scale sediment composition and productivity (e.g., Shuman, 2003), changes in lake level (e.g., Digerfeldt et al., 1992), or dilution by minerogenic material (e.g., Nesje and Dahl, 2001). Chlorin and OM at Hidden Lake are strongly correlated ($r = 0.77$; $p = 0.01$; Fig. 3; Supplementary Fig. 4), but the two datasets do not always covary during the Holocene. In contrast, chlorin and OM at Kelly Lake are only weakly correlated ($r = 0.28$; $p = <0.01$; Fig. 4; Supplementary Fig. 4). These dissimilarities between the chlorin and OM time series at the two lakes (Figs. 3, 4; Supplementary Fig. 5) might result either from different sampling resolution at the two sites, or uncertainties in the age models. The mismatch might also result from differences in the composition or degradational state of OM, which could affect the measured $RABD_{660;670}$ values, or might indicate that OM is sensitive to multiple, lake-specific processes at these sites.

BSi, in turn, might respond to a number of factors in high-latitude lakes, including length of the ice-free season (McKay et al., 2008), nutrient availability (Perren et al., 2017), dilution by minerogenic material (Krawiec and Kaufman, 2014), or changes in water chemistry that cause dissolution (Bradbury et al., 1989). SEM imaging of diatoms in Kelly Lake sediments reveals well-preserved valves, indicating that dissolution is not a factor affecting BSi in this sequence (Supplementary Fig. 2). Fluctuations in BSi and OM at Kelly Lake are not significantly correlated at the 95% confidence level ($r = 0.22$; $p = 0.12$; Fig. 4; Supplementary Fig. 4), indicating either that changes in BSi at this site might be uncoupled from allochthonous OM inputs, or that BSi reflects processes that affect diatoms directly, such as changes in seasonality (Buczkó et al., 2018) or taxon-specific responses of diatoms to changing climate or environmental conditions (Lotter and Hofmann, 2003). However, chlorin and BSi at Kelly Lake are moderately correlated ($r = 0.40$; $p < 0.01$; Fig. 4; Supplementary Fig. 4), indicating that BSi (dominantly composed of diatoms at this site) is an important component of total chlorophyll production in the lake and its catchment, and that BSi is influenced by at least some of the same climate variables that drive overall productivity at both lakes. Similar to diatom abundance (as reflected by BSi), the abundance of bryozoan statocysts in lake sediment can indicate past productivity, where more statocysts occur with higher concentrations of nutrients in the lake water (Crisman et al., 1986; Hartikainen et al., 2009).

Indicators of past vegetation change

Productivity also can be influenced by changes in plant community composition in the Hidden Lake and Kelly Lake catchments. For example, *Alnus* is known to increase local nitrogen availability (Shaftel et al., 2011), and its arrival has been shown to drive increases in BSi at nearby Sunken Island Lake (Broadman et al., 2020) and in southwestern Alaska at Farewell Lake (Hu et al, 2001) and Lone Spruce Pond (Kaufman et al., 2012). These fluctuations in nutrient content associated with shifts in vegetation can also drive changes in diatom assemblages because some diatom species respond strongly to the presence of certain nutrients (e.g., Perren et al., 2017).

Whereas pollen data tend to reflect regional vegetation changes, plant macrofossil data more closely reflect the taxa immediately surrounding the lake (e.g., Jackson et al., 2014). Therefore, the presence of *Picea*, *Alnus*, and *Betula* macrofossils in Kelly Lake sediments confirm the presence of these taxa in the immediate vicinity of this site, while the Hidden Lake pollen record indicates the presence of these taxa over a broader region.

Indicators of past hydroclimate

Several indicators analyzed in this study are commonly used to reconstruct past hydroclimate conditions. For example, the presence of some micro- and macrofossils can indicate changes in lake level, including oospore macrofossils associated with Characean algae (*Chara* sp.). *Chara* is a genus of photosynthetic macrophyte that dwells in shallow, clear waters (typically ∼1–3 m water depth; Pukacz et al., 2016). Large quantities of *Chara* oospores in lake sediment have been associated with dense meadows of *Chara* proximal to the site sampled (Zhao et al., 2006; Ayres et al., 2007), and with the persistent presence of *Chara* over prolonged time periods (Van den Berg et al., 2001). Therefore, an increase in the abundance of *Chara* oospores in Kelly Lake sediments indicates that these algae were more abundant near the coring site at the lake's depocenter. Simple bathymetric modeling (Supplementary Fig. 3) reveals that a decrease in lake level would shift shallower waters closer to this coring site. Therefore, an increase in the concentration of oospores likely reflects a lower lake level at Kelly Lake.

Similarly, the concentration of bryozoan statocysts can indicate lake level. Bryozoans attach themselves to logs and aquatic macrophytes (Francis, 2001; Wood, 2001), and therefore an increase in the concentration of statocysts may reflect a lower lake level at Kelly Lake. An increased concentration of statocysts also can be interpreted to indicate the presence of flowing surface or spring water, which is often (but not always) associated with shallow water (Francis, 2001; Wood, 2001). Diatom assemblages can provide yet another line of evidence for lake level fluctuations, where an increase in the relative abundance of planktonic diatom taxa can indicate a rise in lake level that creates additional habitat for these diatoms (Wolin and Duthie, 1999).

These inferred lake level changes can be interpreted to reflect changes in hydroclimate. For example, a rise in inferred lake level might indicate an increased contribution of groundwater (e.g., from melting glaciers), or an increase in the amount of precipitation relative to evaporation (increased P-E). Precipitation rate and P-E, in turn, are strongly influenced in this region by the strength of the Aleutian Low, where a stronger pressure cell typically
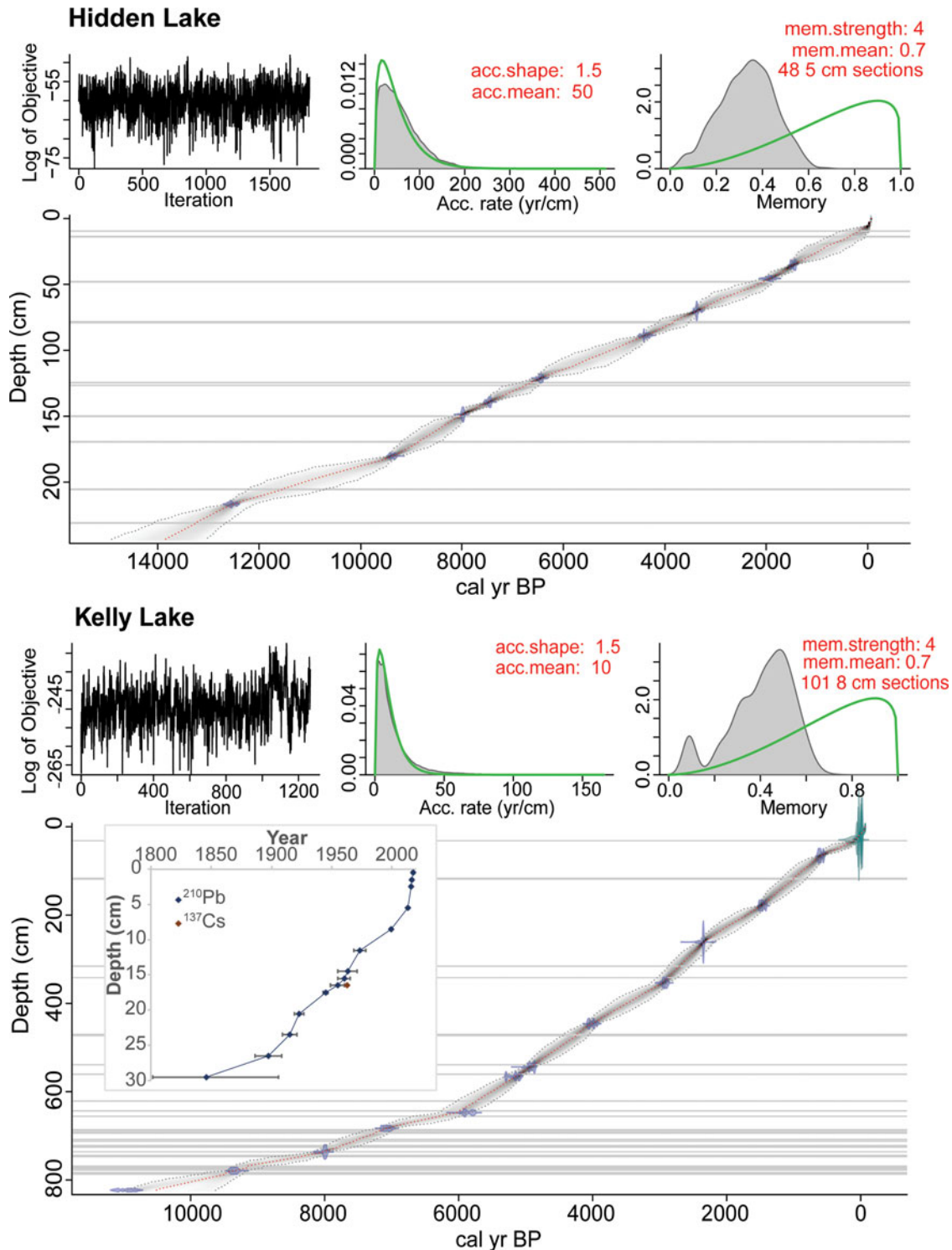
Figure 5. Age-depth models for Hidden Lake core HD14-2 and Kelly Lake core KLY18-2, created using Bacon (v2.2; Blaauw and Christen, 2011). Gray horizontal lines mark visible tephra deposits (as well as large branches in Kelly Lake) that are assumed to have been deposited instantaneously. The depths and basal ages of the tephra layers are in Supplementary Table 3. Inset shows the ^{210}Pb and ^{137}Cs profile of the near-surface sediments from Kelly Lake (data in Supplementary Fig. 2 and Supplementary Table 1).

results in increased storminess and generally wetter winters in southern Alaska (Rodionov et al., 2007).

$\delta^{18}O_{diatom}$ is also sensitive to changes in past hydroclimate. The temperature-dependent fractionation between diatom silica and lake water is relatively small, meaning it is often overwhelmed by larger fluctuations in δ_L that can occur due to changes in P-E, δ_P, or other changes in lake hydrology (see Leng and Barker, 2006) for a summary of the influences on $\delta^{18}O_{diatom}$). This is particularly relevant in the North Pacific region, where relatively large magnitude changes in both P-E and δ_P have been
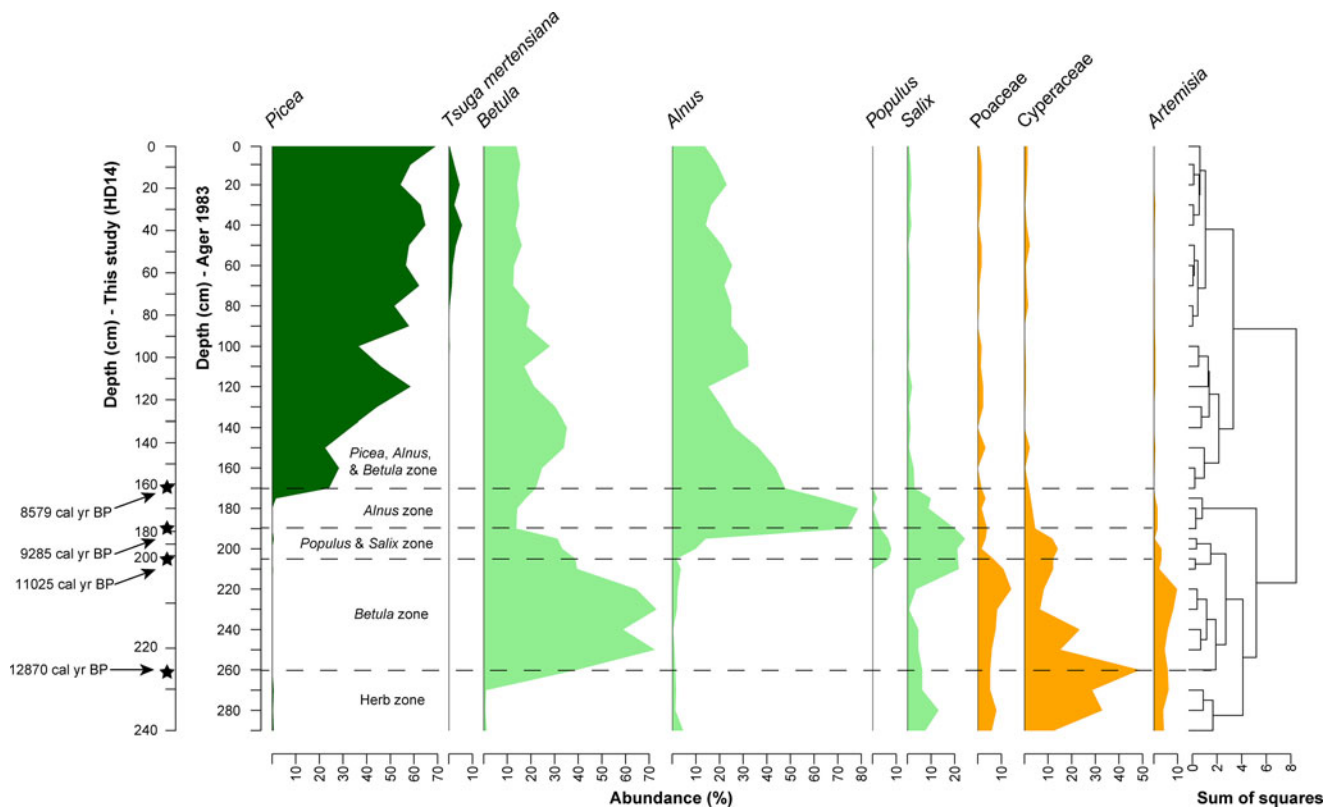
Figure 6. Relative abundance of dominant pollen types in Hidden Lake from Ager (1983), shown alongside new ages and approximate depths associated with the pollen data from core HD14-2 and the corresponding age model shown in Figure 5. Pollen types include conifers (dark green), deciduous trees (pale green), and shrubs and grasses (orange). Dashed lines show the originally identified vegetation zones (Ager, 1983). CONISS-designated clusters are shown on the right. Analyzed and plotted using the R packages Rioja (v.0.9-26; Juggins, 2017) and Vegan (v.2.5-7; Oksanen et al., 2007).

documented during the Holocene. Therefore, $\delta^{18}O_{diatom}$ from Kelly Lake is interpreted primarily in terms of hydroclimatic variables, as has been done for other $\delta^{18}O_{diatom}$ records from southern Alaska (Schiff et al., 2009; Bailey et al., 2015, 2018; Broadman et al., 2020), rather than in terms of Holocene temperature changes.

While P-E and evaporative isotope enrichment are major influences on δ_L in many closed-basin lakes (e.g., Broadman et al., 2020), several lines of evidence suggest their influence at Kelly Lake is minimal in recent years compared with nearby lakes. First, according to a survey of regional water isotopes (Broadman et al., 2020), modern δ_L at Kelly Lake (−13.9‰ VSMOW; $n = 7$) is only slightly elevated above that of local rivers (−14.8‰ and −16.6‰ for the Moose and Kenai rivers), regional groundwater (−16.5‰), and the precipitation-weighted annual average of regional precipitation (−17.7‰, recorded in Anchorage from 2005–2018; Bailey et al., 2019). In contrast, δ_L at many closed-basin lakes in the Kenai lowlands ranges from −10‰ to −6‰ (Fig. 2B). Second, $\delta^{18}O_{diatom}$ values have decreased in recent decades (upper 18 cm of sediment), while annual temperature has increased (Fig. 10H) and average annual precipitation rates have remained constant or slightly decreased since 1940 CE (see data for Kenai airport at https://akclimate.org/data/data-portal/). Were $\delta^{18}O_{diatom}$ sensitive to P-E, this would be the opposite of the pattern that would be expected, because rising temperature leads to increased evaporation, a phenomenon that was documented in the most recent sediments of nearby Sunken Island Lake (Broadman et al., 2020).

Another factor influencing δ_L at Kelly Lake is change in the flux and isotope composition of groundwater (Gi and δ_{Gi}). Several lines of evidence suggest that Gi is an important component of Kelly Lake's hydrological budget, including the presence of visibly discharging subaqueous springs, and a substantial contribution of Gi calculated in the mass balance model output for the modern period (Fig. 9G). In the Kenai lowlands there are two possible sources for Gi: a surficial aquifer and a deep aquifer (Eilers et al., 1992). Geochemical evidence from a survey of lakes in the Kenai lowlands suggests that lakes fed by the deep aquifer have higher alkalinity and total dissolved solids (TDS) compared with lakes fed by the surficial aquifer (Eilers et al., 1992). The presence of carbonate muds (marl) during the late glacial and Early Holocene, as well as relatively high values for limnological indicators analyzed at Kelly Lake in June 2021 (pH: 7.8; conductivity: 144 µm; alkalinity: 62 ppm; total hardness: 62 ppm) suggest that Kelly Lake is fed by relatively deep groundwater. Furthermore, similar but slightly higher values for all indicators analyzed at Hidden Lake (pH: 8.3; conductivity: 183 µm; alkalinity: 75 ppm; total hardness: 78 ppm) indicate this groundwater might travel to Kelly Lake via Hidden Lake. Deep groundwater is likely recharged by snowmelt at high altitudes in the Kenai Mountains, and thus is primarily fed by winter season precipitation, which has low $\delta^{18}O$ (Fig. 2A). In addition to climatic fluctuations that could influence Gi, groundwater sourced from a deep aquifer also could be influenced by tectonic activity because Kelly Lake is located proximal to a fault that lies along the mountain front (Karlstrom, 1964). The influence of tectonism on
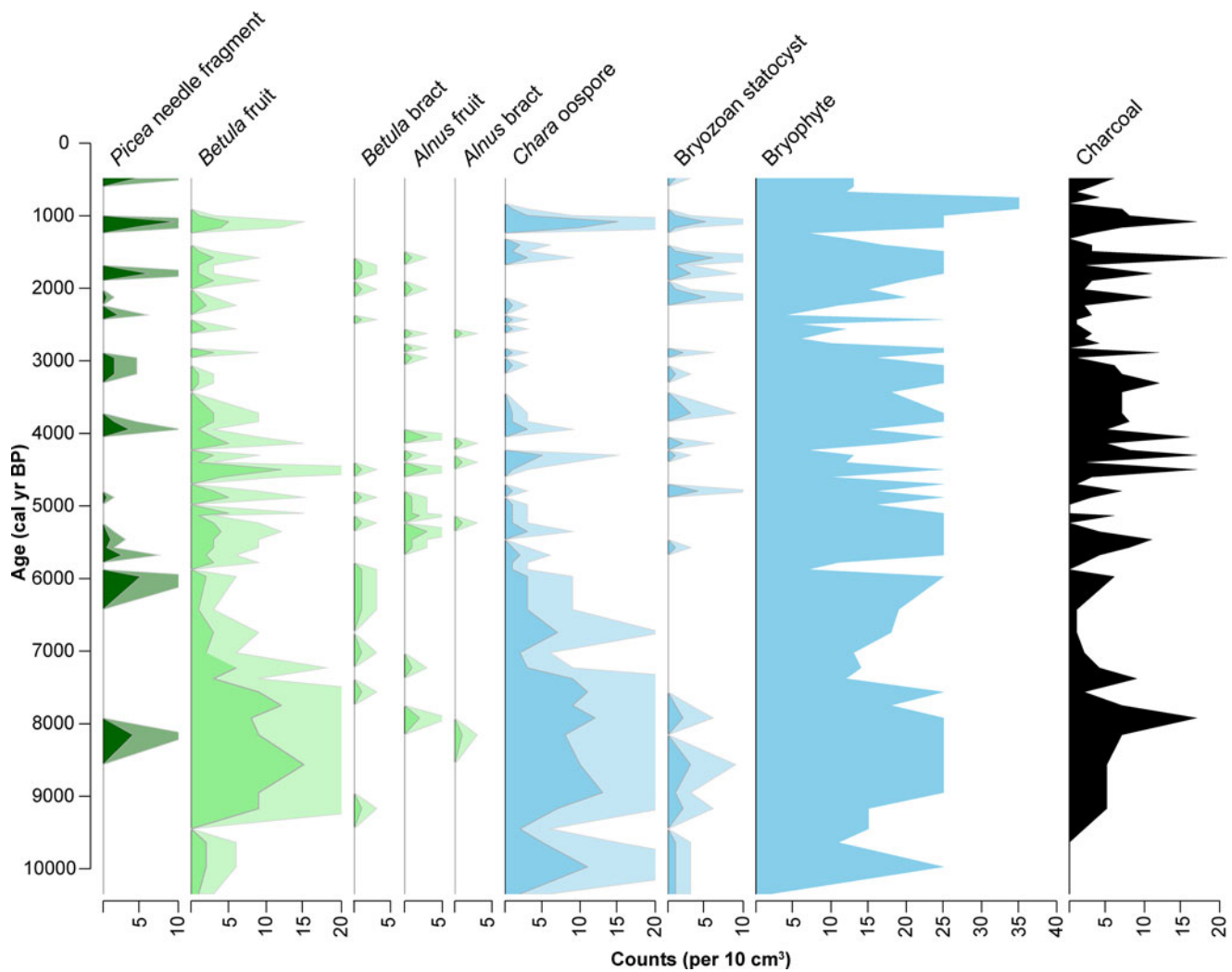
Figure 7. Concentration of terrestrial (green), aquatic (blue), and charcoal macrofossils identified in Kelly Lake core KLY18-2. Analyzed and plotted using the R package Rioja (v.0.9-26; Juggins, 2017). Pale shading is a 3x exaggeration of the actual concentration.

groundwater discharge has been demonstrated at other lakes adjacent to fault zones (e.g., Hosono et al., 2020; Ide et al., 2020).

It is also possible that Kelly Lake is fed by surficial groundwater, which is likely recharged in part by glacier meltwater. Studies examining glacier retreat during recent decades have demonstrated that the meltwater generated by receding glaciers can recharge a surface aquifer and form an important component of lowland river discharge, even as glacier ice retreats into the mountains (e.g., Liljedahl et al., 2017). Continental ice tends to incorporate primarily snowfall that fell at high elevation (Fig. 2A), and therefore glacier ice can be expected to have relatively low $\delta^{18}O$ (e.g., Bhatia et al., 2011). Therefore, during periods of glacial retreat, it is likely that surficial groundwater in the Kenai lowlands would have relatively low $\delta^{18}O$. If Kelly Lake is currently or was previously fed by the surficial aquifer, glacial meltwater might contribute substantially to Gi at this site during periods of glacier retreat. However, a physical connection between the surficial aquifer and the Kelly Lake subaqueous springs remains uncertain, limiting our ability to definitively identify the source of Gi (surficial or deep).

Regardless of the mechanism(s) influencing Gi at this site, it is likely that δ_{Gi} at Kelly Lake would be relatively low, both now and in the past, because both the deep and surficial groundwater in the region are recharged by sources at high elevations that dominantly incorporate winter precipitation. This is supported by the $\delta^{18}O$ of local well water (-16.5‰), which is lower than the modern δ_L of Kelly Lake (-13.9‰) (Fig. 2B; Broadman et al., 2020). Therefore, increased Gi would likely decrease δ_L at Kelly Lake.

Both δ_{Gi} and δ_L are also sensitive to changes in δ_P, which is influenced by seasonal changes in air temperature (Dansgaard, 1964) (Fig. 2A) and the trajectories of storms that deliver precipitation (e.g., Bailey et al., 2015). In south-central Alaska, summer season (JJA) precipitation tends to have higher δ_P values, whereas the winter season (DJF) has lower δ_P (Fig. 2A). Therefore, a shift in the seasonality of precipitation (e.g., a larger proportion of annual precipitation falling in the summer) would influence annually weighted δ_P, as well as the contribution of δ_{Gi} derived from recent precipitation, and would subsequently change δ_L.

The other important influences on δ_P in this region are the source area and trajectory of storms, which are controlled by the position and intensity of the Aleutian Low (AL). Because a strong AL encourages south-to-north (meridional) transport from the Gulf of Alaska to the Kenai lowlands (Cayan and
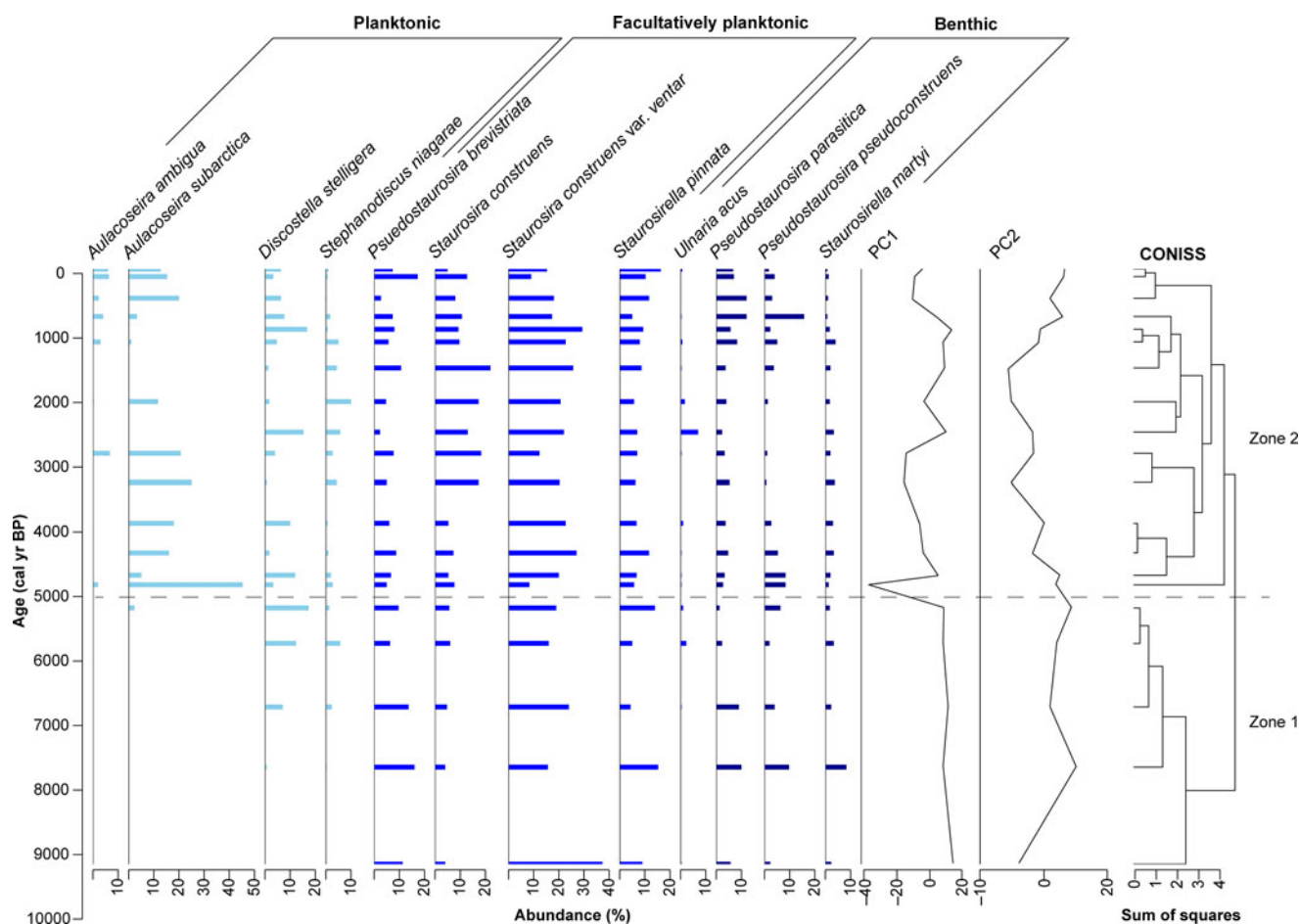
Figure 8. Relative abundances of 12 dominant diatom taxa in Kelly Lake core KLY18-2. CONISS-designated zones are indicated by the dashed line. Analyzed and plotted using the R packages Rioja (v.0.9-26; Juggins, 2017) and Vegan (v.2.5-7; Oksanen et al., 2007).

Peterson, 1989; Mock et al., 1998; Rodionov et al., 2007; Berkelhammer et al., 2012), storms associated with a strong AL tend to travel less distance and cross fewer continental barriers before arriving in the Kenai lowlands. Conversely, a weak AL encourages west-to-east (zonal) transport from farther west in the North Pacific Ocean. Storms during a weak AL tend to travel greater distances and cross more continental barriers, and therefore are likely to experience more rain-out of ^{18}O, depleting δ_P arriving in the Kenai lowlands. This relationship between the AL and δ_P has been corroborated by several isotope-enabled model experiments (Berkelhammer et al., 2012; Porter et al., 2014).

In contrast, some authors have suggested the opposite relationship, where a stronger AL results in lower δ_P. However, studies that invoke this opposing relationship between δ_P and AL strength have attributed it to unique characteristics of their study sites, such as a strong rain-out effect (Anderson et al., 2005), high altitude (Fisher et al., 2008), or sensitivity to summer conditions (Jones et al., 2014). Furthermore, the limited available modern δ_P data from Anchorage (Bailey et al., 2019) indicates that stronger AL years between 2005 and 2018 had higher δ_P than weak AL years (Broadman et al., 2020). Therefore, we interpret that a stronger AL most likely results in higher δ_P values on decadal to multimillennial timescales at our site. However, the relationship between the AL and δ_P is superimposed on other hydroclimatic

influences (e.g., P-E, seasonality, melting glacier ice), making it difficult to disentangle the influence of AL behavior both in modern δ_P (Bailey et al., 2019) and in paleo oxygen isotope datasets (Broadman et al., 2020) in this region.

As a result of the presence of multiple hydroclimatic variables that influence δ_L and $\delta^{18}O_{diatom}$ at Kelly Lake, the scenarios simulated with the mass balance model include a range of possible values for δ_P, δ_{Gi}, P, and E (Fig. 9A–E). By modeling sensitivity of the system to ranges of values for all these variables, we are able to assess their influence on changes to Gi.

Deglacial and Holocene landscape, vegetation, and hydroclimatic change

Deglaciation and the earliest Holocene (ca. 13.1–9.0 cal ka BP)
The new age model presented in this study places the transition from glaciolacustrine sediments to gyttja in Hidden Lake (Fig. 3) at ca. 13.1 cal ka BP, ca. 3500 years later than suggested by the previously acquired radiocarbon age (Ager, 1983). This stratigraphic transition is associated with retreat of glaciers from the Hidden Lake catchment, and previously has been cited as the termination of the Skilak stade of the Naptowne glaciation, with the Elmendorf stade following shortly thereafter (Fig. 1C; Reger et al., 2007). Moraines previously thought to correlate with the Elmendorf stade lie immediately up valley from

Hidden Lake (Fig. 1C; Reger et al., 2007). However, the absence of glaciolacustrine deposits in the Hidden Lake sediments after ca. 13.1 cal ka BP suggests these presumed Elmendorf-age moraines were formed earlier. A recently revised chronology of the Elmendorf moraine near Anchorage suggests that ice receded from the Matanuska and Knik valleys in two stages: the first between ca. 16.8–16.4 cal ka BP, and the second concluding by ca. 13.7 cal ka BP (Kopczynski et al., 2017). It is possible the moraines in our study region (Fig. 1C) represent a similar progression of events, with the second phase of ice retreat concluding by ca. 13.1 cal ka BP, ending the deposition of glaciolacustrine sediment at Hidden Lake. Because the recovered Hidden Lake sediments terminate in glaciolacustrine silt and sand (rather than till or bedrock), we cannot definitively say whether these sediments at the ca. 13.1 cal ka BP age correspond to termination of the Skilak stade, or a time period thereafter when glaciers were upvalley in Hidden Lake's catchment.

Though a vegetation transition occurs during the Younger Dryas, characterized by a rise in *Betula* and a decrease in Cyperaceae (Fig. 6), there is no evidence for a substantial climate perturbation reflected in the Hidden Lake sedimentological indicators at this time. Therefore, if glaciers in the Kenai Mountains advanced during the Younger Dryas, they were not extensive enough to re-encroach into the Hidden Lake catchment. It is also possible that the influence of groundwater sourced from retreating glaciers at this location near the Kenai Mountains would mask changes documented at nearby sites during the Younger Dryas, as these fluctuations are mostly associated with precipitation and/or atmospheric circulation patterns (e.g., Yu et al., 2008; Kaufman et al., 2010; Broadman et al., 2020).

As arboreal taxa increased from ca. 12.8–9.3 ka cal BP following the retreat of glaciers (Figs. 6, 7), charcoal in the Kelly Lake sediment sequence (Fig. 7) indicates the occurrence of fire that accompanied these developing forests (e.g., Anderson et al., 2006), likely driven in part by warmer summer temperatures (Clegg et al., 2011). Throughout this interval, sediments are composed of interbedded gyttja and gray silt and clay (Fig. 3). These lines of evidence coupled with low values for productivity proxies (chlorin and OM; Fig. 3) suggest a postglacial landscape characterized by low productivity, potentially driven by relatively cool temperatures caused by cold, glacially derived groundwater inputs.

The oldest sediments in Kelly Lake core KLY18-2, which span ca. 10.7–9.2 cal ka BP, are rich in both OM and carbonate (see Wrobleski, 2021, for a detailed description of the carbonate deposits at Kelly Lake). The presence of numerous *Chara* oospores (Figs. 4, 7, 10F) indicates that at least some of the carbonate production at this time was *Chara*-mediated. This profusion of oospores also suggests that *Chara* plants were present in high abundances near the coring location at this time (Zhao et al., 2006). The abundance of *Chara* oospores also indicates that Kelly Lake's water level was lower than present, including at the coring location (Supplementary Fig. 3), because the distribution of *Chara* species in a lake is typically limited to shallow waters (Pukacz et al., 2016). The presence of bryozoan statocysts in the macrofossil assemblage at this time also suggests low lake level (Francis, 2001; Wood et al., 2001).

These findings are consistent with evidence for lowered lake level in the Early Holocene based on dated transitions between minerogenic sediments and terrestrial peat at Sunken Island Lake, 28 km to the northwest (Broadman et al., 2020; Berg et al., in press). In light of these lines of evidence, in our sensitivity

tests for this climate interval, we estimate that Kelly Lake's water level and surface area were reduced, but were still high enough to account for the continuous sediment deposition observed at the coring site of KLY18-4 (Fig. 1D; Table 2; Supplementary Fig. 3). High OM, but low chlorin and BSi, might indicate low productivity in the lake, but with significant allochthonous organic inputs from the *Betula*-dominated hardwood forest, as indicated by the Kelly Lake macrofossil data (Fig. 7) and the Hidden Lake pollen data (Fig. 6). The oldest sample with well-preserved diatoms at ca. 9.2 cal ka BP is dominated by facultatively planktonic taxa, which previously have been shown to thrive in Early Holocene Arctic lakes, possibly due to elevated summer air temperature (Finkelstein and Gajewski, 2008).

The oldest $\delta^{18}O_{diatom}$ samples, from ca. 9.7–9.2 cal ka BP, have the lowest values recorded in the time series (mean = +22.9‰, n = 3), indicating a commensurately low δ_L value (∼ −15.7‰; Table 2). Hydrologic and isotope mass balance modeling suggests two δ_P scenarios that could result in this δ_L value: (1) low δ_P, which might reflect either a weaker AL or a greater annual contribution of winter season precipitation, and less groundwater inflow (Fig. 9D); or (2) δ_P values similar to today's, with similar or larger groundwater inflows (Fig. 9E). Paleoclimate reconstructions also generally indicate δ_P lower than or similar to modern in the Early Holocene (Jones et al., 2014, 2019; Bailey et al., 2018).

While it is not possible to definitively exclude any of these scenarios, it is most likely that δ_P was similar to today (−17.7‰; Bailey et al., 2019), and Gi was similar to its current rate (Fig. 9E). In modeled scenarios where δ_P is substantially lower compared to today (Fig. 9D), P must be ∼25% lower (or evaporation must be ∼25% higher) than that simulated by HadCM3. The 9 ka snapshot already simulates a ∼15% decrease in P during the Early Holocene relative to the modern period (Table 3), and it is unlikely that P would be reduced an additional 25% compared to the model simulation. A scenario with lower δ_P also would require much lower Gi compared to today (Fig. 9D), which is unlikely given the recently deglaciated landscape and likely continued contribution of glacially derived water. Therefore, it is most likely that δ_P was similar to that of today, P was similar to or slightly reduced from the Early Holocene model simulated value, and Gi was similar to that of today (Figs. 9E, 10A–C). δ_{Gi} was probably similar to or lower than δ_P, potentially due to an elevated contribution of meltwater from snow or glacier ice recharging Kenai lowland aquifers following deglaciation (Figs. 9E, 10A–C).

The Early to Middle Holocene transition (ca. 9.0–7.0 cal ka BP)
After the postglacial period characterized by low lake level, groundwater likely sourced from glacial meltwater, and relatively low lacustrine productivity, the following two millennia were transformative. At Kelly Lake, BSi increases over this interval (Fig. 4), coincident with the expansion and dominance of *Alnus* in the region, with the highest relative abundances at ca. 9.3–8.6 cal ka BP (Figs. 6, 10D). The increase in BSi might be driven by the presence of *Alnus* in the Kelly Lake catchment, resulting in nitrogen fixation, more available nitrogen, and consequent diatom blooms (e.g., Perren et al., 2017; Broadman et al., 2020). Though *Alnus* macrofossils do not appear in the Kelly Lake sediments until ca. 8.2 cal ka BP (Fig. 7), the regional increase in *Alnus* (Fig. 6) coupled with the increase in BSi (Fig. 10D) indicates a relationship between the two at Kelly Lake. The diatom assemblage remains dominated by facultatively planktonic taxa (Fig. 8), and *Chara* oospores and bryozoan statocysts remain
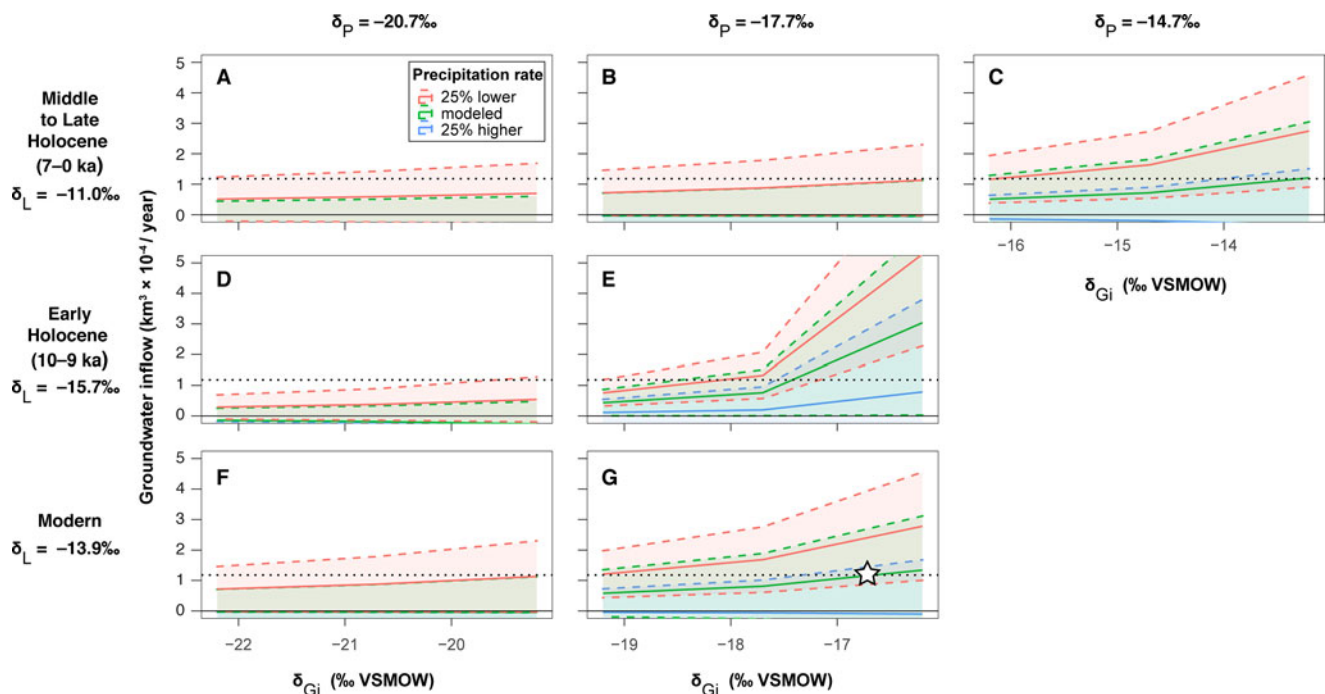
Figure 9. Output of sensitivity tests conducted to investigate past hydrologic and isotope mass balance at Kelly Lake. (**A–C**) Middle to Late Holocene scenarios (HadCM3 4 ka snapshot). (**D, E**) Early Holocene scenarios (HadCM3 9 ka snapshot). (**F, G**) Modern scenarios. (**A, D, F**) Scenarios where precipitation and groundwater oxygen isotope values are lower compared with today. (**B, E, G**) Scenarios where precipitation and groundwater oxygen isotope values are similar to today. (**C**) Scenario where precipitation and groundwater oxygen isotope values are higher than today (this scenario is feasible only in the Middle to Late Holocene). Blue lines and shading show scenarios where *P* is 25% higher compared to the HadCM3 output; green shows *P* that is the same as the HadCM3 output; and pink shows *P* that is 25% lower. Solid blue, green, and pink lines show these *P* scenarios with the same evaporation rate as the HadCM3 output, whereas upper and lower bounds (dashed lines) show scenarios where *E* is reduced or increased 25% compared to the HadCM3 output. In all panels, the black dotted lines show the calculated groundwater inflow for the modern period (1.2×10^{-4} km³/year). The white star in (**G**) indicates the values of *P*, *E*, groundwater inflow, groundwater oxygen isotopes, and precipitation oxygen isotopes calculated using the modern measurements.

relatively abundant (Fig. 10F, G), suggesting there was little change in lake level over this interval.

$\delta^{18}O_{diatom}$ increases over this interval by ∼5‰ (from + 22.9‰ prior to 9 cal ka BP to + 27.9‰ during the two millennia starting at 7 cal ka BP), indicating a transition either in the lake's hydrologic inputs (e.g., precipitation or groundwater) or in regional hydroclimate. The cause of the transition between ca. 9–7 cal ka BP is likely associated with a change in *Gi* and δ_{Gi}, potentially due to the decreased influence of meltwater from retreated glaciers by ca. 7 cal ka BP. Because Kelly Lake lies close to the mountains (Fig. 1C), it might be more strongly influenced by glacier melt compared with sites further north or west in the Kenai lowlands. Kelly Lake's proximity to the mountains relative to these other sites might explain the lack of evidence for a shift in hydrology or hydroclimate at this time in nearby oxygen isotope reconstructions (e.g., Jones et al., 2014, 2019; Broadman et al., 2020). This possibility is supported by the Middle to Late Holocene model scenarios, which require lower *Gi* compared to the present (Fig. 9A–C).

The diminished influence of groundwater would have resulted in a lower water table and less saturated soils, which might help explain the establishment and expansion of *Picea* near Hidden and Kelly lakes in the Early Holocene. *Picea glauca* (white spruce) is the *Picea* species that most likely arrived initially, as documented in many nearby locations at this time (Anderson et al., 2006, 2017, 2019). The first occurrence of *Picea* macrofossils at Kelly Lake (ca. 8.2 cal ka BP; Fig. 7) occurs approximately concurrent with that recorded at other locations in the Kenai lowlands,

suggesting that migration of *P. glauca* is regionally consistent; however, the transition to a *Picea*-dominated forest (by ca. 8.0 cal ka BP; Fig. 6) occurs substantially earlier (e.g., Anderson et al., 2006, 2017, 2019). *Picea glauca* does not tolerate saturated soils (Landhausser et al., 2003), and it has been suggested that it will not become established until soil properties, including soil moisture, are sufficient for it to succeed (Henne et al., 2011). Therefore, the relatively early transition to a *Picea*-dominated forest might be explained in part by a shift in soil properties (i.e., less water-logged soils) driven by a reduction in *Gi*. Once established, *P. glauca* likely affected soil properties (Messender, 1980; Ranger and Nys, 1994; Orlova et al., 2016), potentially creating a positive feedback between *Picea* expansion and soil development.

Rising lake level during the Middle Holocene (ca. 7.0–5.0 cal ka BP)

Following the preceding transition in lake hydrology and soil development, proxy data suggest lake level at Kelly Lake may have risen from ca. 7.0– 5.0 cal ka BP, in agreement with conclusions based on other sites in this region (Kaufman et al., 2016; Broadman et al., 2020; Berg et al., in press). While most sedimentological data indicate little change occurred at this time (Figs. 3, 4), by 5 cal ka BP there is an increase in the proportion of planktonic diatoms (Fig. 10E), which might reflect an increase in available water column habitat caused by rising lake level (Wolin and Duthie, 1999). At the same time, concentrations of *Chara* oospores and bryozoan statocysts decline, with low concentrations prevailing during the Late Holocene starting at ca. 5 cal ka BP
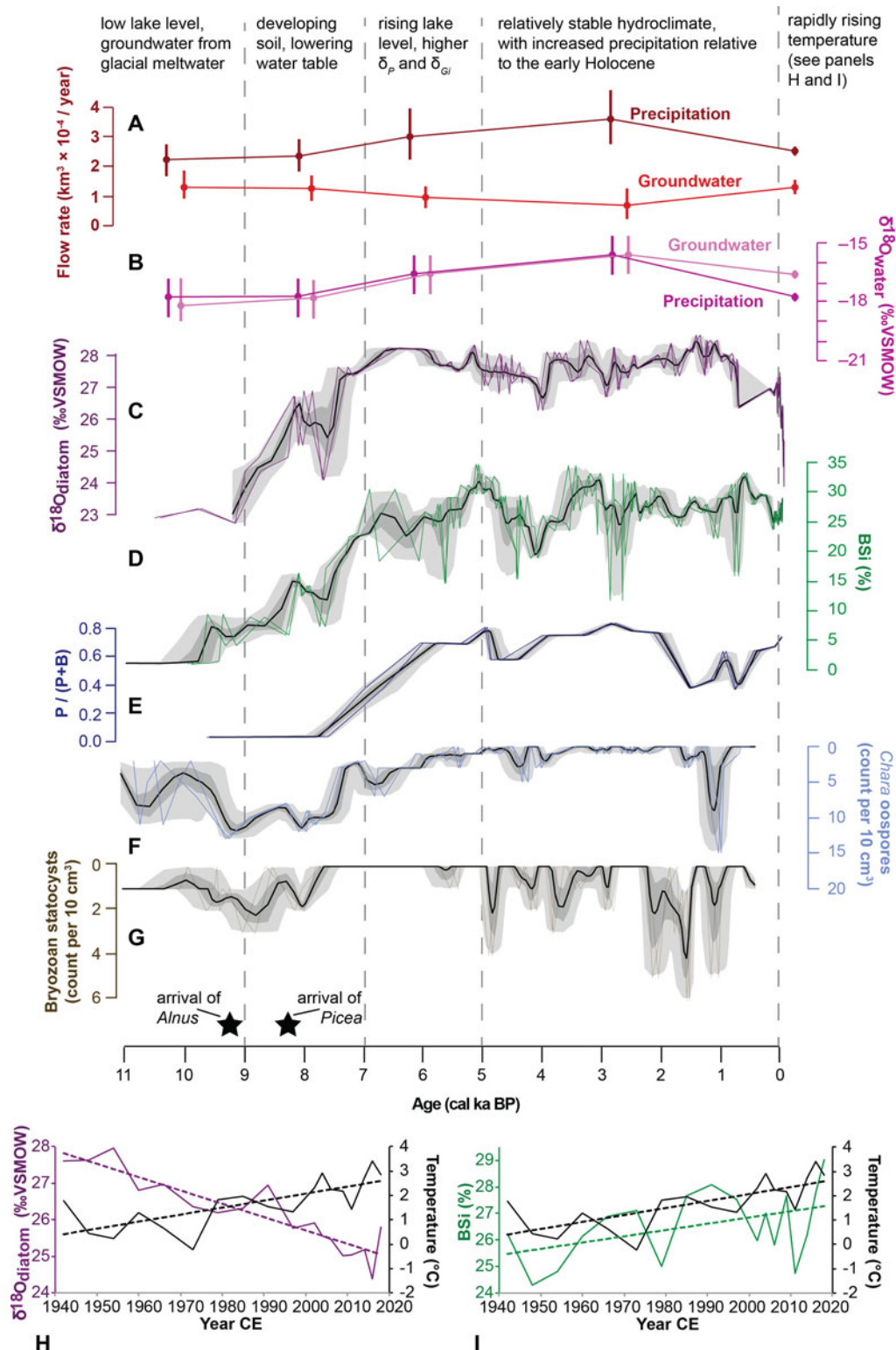
Figure 10. Summary of key hydroclimate indicators from Hidden and Kelly Lakes. (**A, B**) Most plausible modeled scenarios (Fig. 9) for each time period for: (**A**) rates of groundwater inflow and precipitation, and (**B**) oxygen isotope composition for each of these hydrologic inputs to Kelly Lake. Vertical bars are uncertainty estimates, some of which are based on measurements, and some of which are simulated or inferred. (**C–G**) Ribbon plots of proxy data from Kelly Lake; black lines are the mean of the age model ensembles, dark- and light-gray shading encompass 68% and 95% of the ensemble members, respectively; colored lines show five representative members of the age model ensemble. Ribbon plots show the following datasets: (**C**) $\delta^{18}O_{diatom}$ (‰ VSMOW); (**D**) BSi (%); (**E**) proportion of planktonic diatoms, calculated as the number of planktonic diatoms (P) divided by the sum of all planktonic and benthic diatoms (P + B); (**F**) concentration of *Chara* oospores (count per 10 cm³); and (**G**) concentration of bryozoan statocysts (count per 10 cm³); the first occurrences of *Alnus* and *Picea* macrofossils at Kelly Lake are shown (black stars). (**H**) Temperature at Kenai airport (black) shown with Kelly Lake $\delta^{18}O_{diatom}$ (purple) data from 1944–2018 CE, with linear trend lines. (**I**) Temperature at Kenai airport (black) shown with Kelly Lake BSi (green) abundance from 1944–2018 CE, with linear trend lines. The age-uncertain correlations for data in **B** and **C** are shown in Supplementary Figure 5.

(Fig. 10F, G). While likely related to rising lake level, we suggest that the decline of *Chara* might also have been driven by a decrease in pH associated with establishment of coniferous forest. Following these lines of evidence, and because satellite imagery reveals that lake level was higher compared to modern conditions at some point in the past (Supplementary Fig. 3), sensitivity tests for the Middle to Late Holocene (Fig. 9A–C) assume lake level was slightly higher compared to modern conditions.

$\delta^{18}O_{diatom}$ (average = +27.9‰, n = 14) and inferred δ_L values are elevated compared to previous millennia, and fluctuate relatively little over this 2000 year period, despite evidence for rising lake level. Due to the diminished influence of groundwater sourced from retreating glaciers, the dominant controls on δ_L likely shifted to P, E, and δ_P. Results of the sensitivity tests suggest that high δ_L could plausibly have resulted from δ_P either higher than (Fig. 9C) or similar to (Fig. 9B) that of today. A scenario with higher δ_P requires wetter conditions than simulated by HadCM3 (Fig. 9C), whereas scenarios with lower δ_P require drier conditions (Fig. 9A, B). Reconstructions from nearby sites suggest δ_P remained relatively low at ca. 7 cal ka BP, but increased by ca. 5–4 cal ka BP (Jones et al., 2014, 2019; Bailey et al., 2018; Broadman et al., 2020). A synthesis of hydroclimate records from this region also indicates that southern Alaska became wetter during the Late Holocene, compared with a relatively drier Middle Holocene (Kaufman et al., 2016). Therefore, it is likely that δ_P was similar to modern, and P was relatively low at ca. 7 cal ka BP, but that both began to increase by ca. 5 cal ka BP (Figs. 9C, 10A–C).

High lake level and relative stability during the Late Holocene (ca. 5.0–0 cal ka BP)

Relatively high δ_P and increased P (Fig. 9C) likely persisted for much of the Late Holocene. $\delta^{18}O_{diatom}$ values during the most recent ca. 5 cal ka BP exhibit relatively little variability (mean = +27.6‰; n = 66), and inferred lake level is stable compared to previous millennia (Figs. 4, 10E–G). Continued relatively high $\delta^{18}O_{diatom}$ (and therefore δ_L) over this time period might be driven by increased δ_P associated with a strengthened AL, which has been documented in previous studies to begin at ca. 5.5–4.5 cal ka BP (Jones et al., 2014, 2019; Bailey et al., 2018; Broadman et al., 2020; Du et al., 2020).

An increase in the abundance of both BSi and bryozoan statocysts (Fig. 10D, G) at this time might indicate increased productivity and nutrient concentrations in Kelly Lake (Crisman et al., 1986; Hartikainen et al., 2009; Perren et al., 2017). Additionally, the increased concentration of bryozoan statocysts and, to a lesser extent, *Chara* oospores (Fig. 10F, G), might have resulted from an increase in lake level that inundated the shallowest area of Kelly Lake (Supplementary Fig. 3), creating additional habitat for these organisms that are limited to shallow waters (Francis, 2001; Wood, 2001; Pukacz et al., 2016). Composition of the surrounding vegetation (Figs. 6, 7) and indicators of both productivity (Figs. 3, 4) and lake level (Fig. 10E–G) remain relatively stable throughout the Late Holocene.

Whereas many paleo isotope datasets from southern Alaska show one of the largest step-shifts and/or changes in variability during the Middle to Late Holocene transition, or during the Late Holocene (e.g., Schiff et al., 2009; Jones et al., 2014, 2019; Bailey et al., 2018; Broadman et al., 2020), this is not the case for Kelly Lake. Here, the largest step shift prior to the instrumental period occurs from the Early to Middle Holocene (Fig. 10C). This pronounced difference might indicate the importance of

Gi and δ_{Gi} in influencing δ_L at Kelly Lake, due to its location adjacent to mountains and glaciers. Furthermore, the Kelly Lake proxy data do indicate that lake level increased by ca. 5 cal ka BP, suggesting a hydroclimatic and/or hydrologic shift may have occurred at this time (Fig. 10E–G), likely associated with shifts in P, E, and δ_P (rather than by changes in Gi and δ_{Gi}). Overall, it is most likely that the influence of a strengthened AL by ca. 5–4 cal ka BP that dominates the Holocene oxygen isotope datasets from several nearby sites is subdued in this $\delta^{18}O_{diatom}$ dataset due to Kelly Lake's hydrologic setting.

Abrupt change in recent decades (1950 CE–present)

While most datasets analyzed in this study do not extend through recent decades, or do not have sufficient temporal resolution to examine trends over the instrumental period, both BSi and $\delta^{18}O_{diatom}$ values at Kelly Lake do have sufficient resolution for this, and show abrupt changes since ca. 1950 CE. Specifically, BSi increases from 1944–2018 CE (average = 26.7%, n = 16; Fig. 10I), whereas $\delta^{18}O_{diatom}$ decreases over this time period, to values approaching those of the earliest Holocene (average = +25.5‰, n = 16; Fig. 10H). These trends in $\delta^{18}O_{diatom}$ and BSi coincide with rapidly increasing temperature at Kenai airport (Fig. 10H, I; https://akclimate.org/data/data-portal/). To compare these temperature data with the proxy data time series, the daily measurements were compiled into annual averages, and age-uncertain correlations were performed using geoChronR (v.1.0.6; McKay et al., 2021). Data were binned into 2-year intervals and then corrected for both autocorrelation (using "isospectral" significance testing; Ebisuzaki, 1997) and a false discovery rate (FDR; Ventura et al., 2004). These analyses reveal that $\delta^{18}O_{diatom}$ is negatively correlated with temperature over this period (median $r = -0.54$; $p < 0.05$ for 100% of ensembles; Supplementary Fig. 5), though BSi is not significantly correlated with temperature (Supplementary Fig. 5). However, the linear trends (Fig. 10H, I) indicate that both sets of proxy data generally covary with temperature over this interval.

Rising temperature has affected the Kenai Peninsula in numerous ways (Hayward et al., 2017) and might have had direct effects on these two paleoenvironmental indicators. For example, the timing of ice-out strongly depends on air temperature throughout Alaska (Arp et al., 2013). Therefore, rising air temperatures over recent decades in the Kenai lowlands very likely has reduced the duration of perennial lake ice cover, as has been demonstrated at a circum-Arctic scale (Šmejkalová et al., 2016). This would lengthen the growing season, encouraging diatom blooms that cause increased BSi.

As described previously, the direct influence of temperature on $\delta^{18}O_{diatom}$ tends to be subsumed by larger fluctuations in hydroclimatic variables (Leng and Barker, 2006). However, this decrease in $\delta^{18}O_{diatom}$ could be driven in part by rising air temperature and the resulting effect on δ_P (Dansgaard, 1964), or might reflect indirect effects of rising temperature, such as an increased contribution of glacially derived groundwater, or an increase in the relative contribution of winter precipitation. Rising temperature has caused glaciers to retreat rapidly in the nearby Kenai Mountains (Hayward et al., 2017), potentially resulting in an increased relative proportion of glacial meltwater in the surficial groundwater that might feed Kelly Lake (e.g., Liljedahl et al., 2017). Rising temperatures have also caused a reduction in the extent and annual duration of sea ice in Cook Inlet (NSIDC, 2018), potentially leading to an increased contribution of winter season precipitation with low δ_P values. This relationship between

Cook Inlet sea ice cover and δ_P has been previously documented in Anchorage (Bailey et al., 2019).

These rapid, recent changes, which occur following ca. 7000 years of relative stability in both proxy datasets, indicate that anthropogenic climate change is drastically altering the hydrology and productivity of Kelly Lake, demonstrating the sensitivity of this site to global warming. The recent decrease in $\delta^{18}O_{diatom}$ values also highlights that Kelly Lake's current and future hydrologic balance may be more similar to that of the Early Holocene than much of the last ca. 7000 years. Though some hydrologic inputs differ between the Early Holocene and today (e.g., precipitation seasonality and AL strength), the increased influence of *Gi* driven by melting snow or glacier ice in both time periods may be sufficient to dominate δ_L and $\delta^{18}O_{diatom}$.

CONCLUSIONS

The data presented in this study reveal a dynamic deglacial and Holocene hydrologic and environmental history at Hidden and Kelly lakes. An updated chronology for sediment accumulation shows that Hidden Lake was deglaciated by ca. 13.1 cal ka BP; this minimum age for deglaciation is ca. 3500 years younger than the previously reported minimum age (Ager, 1983). Glacial meltwater that likely recharged aquifers during the Early Holocene was likely a key component in the hydrological budget of Hidden and Kelly lakes, due to their mountain-adjacent locations. From ca. 7–5 cal ka BP, lake level at Kelly Lake rose, possibly due to increased precipitation associated with a strengthening AL. By 5 cal ka BP, lake level likely had reached or exceeded its modern level. Elevated lake level persisted throughout the Late Holocene, likely due to sustained, increased precipitation and a strong AL, which has been documented throughout southern Alaska and southeastern Yukon. Since the 1940s, rapid changes in BSi and $\delta^{18}O_{diatom}$ indicate that rising temperatures have altered the Kelly Lake ecosystem, likely due to reduced seasonal ice cover in both the lake and nearby Cook Inlet, and possibly an increased contribution of glacial melt in the groundwater that feeds Kelly Lake. These results demonstrate the vulnerability of this region to climate change, and suggest that warming-related perturbations are causing dramatic changes following ca. 7000 years of relatively stable climate conditions.

Our results reveal a site-specific response to Late Pleistocene and Holocene environmental change in the Kenai lowlands, characterized in part by the importance of groundwater sourced from snow or glacier ice, both during the Early Holocene and in recent decades. Our findings also demonstrate that a multi-lake, multi-proxy approach complemented by simple quantitative modeling can be useful in reconstructing past hydroclimatic change. For example, output from the mass balance modeling experiments provide estimates for past groundwater and meteoric inputs to Kelly Lake at a multi-millennial timescale (Fig. 10A, B), and the diatom assemblage and macrofossil data reflect changes in past lake level (Fig. 10E–G). We have also demonstrated that Kelly Lake $\delta^{18}O_{diatom}$ (Fig. 10C) represents the integrated influence of multiple controls on δ_L, and that this dataset cannot be interpreted in terms of a single hydroclimate variable. As such, the results from this study reinforce four recommendations pertinent to interpreting lacustrine paleo oxygen isotope data. (1) Simple hydrologic and isotope mass balance models can be effective in complementing and constraining interpretations derived from proxy-based isotope data, and can help identify the most likely scenario out of many possibilities. (2) Examining numerous proxies in neighboring lakes can

yield a more complete understanding of past hydrologic and environmental change, as opposed to relying on a single site or single dataset that might be disproportionately influenced by site- or proxy-specific characteristics. (3) Inflow rates and isotope composition of groundwater can be major influences on lake water isotope composition, both now and in the past. The role of groundwater may be particularly important in lowland regions adjacent to mountain glaciers, and might be a more influential component of hydrologic and isotope mass balance than is generally considered for lake-sediment-based paleo isotope datasets. (4) Even where regional or synoptic scale climate influences are thought to dominate Holocene hydroclimate (e.g., Aleutian Low variability), site-specific responses can yield unexpected and counter-intuitive results. As such, investigators must consider how site-specific responses might confound regional climate influences.

Competing Interests Statement. The authors declare that they have no conflict of interest.

REFERENCES

Ager, T.A., 1983. Holocene vegetational history of Alaska. In: Wright, H.E. (Ed.), *Late Quaternary Environments of the United States, vol. 2.* University of Minnesota Press, pp. 128–141.

Anderson, L., Abbott, M.B., Finney, B.P., Burns, S.J., 2005. Regional atmospheric circulation change in the North Pacific during the Holocene inferred from lacustrine carbonate oxygen isotopes, Yukon Territory, Canada. *Quaternary Research* **64**, 21–35.

Anderson, L., Abbott, M.B., Finney, B.P., Burns, S.J., 2007. Late Holocene moisture balance variability in the southwest Yukon Territory, Canada. *Quaternary Science Reviews* **26**, 130–141.

Anderson, L., Birks, J., Rover, J., Guldager, N., 2013. Controls on recent Alaskan lake changes identified from water isotopes and remote sensing. *Geophysical Research Letters* **40**, 3413–3418.

Anderson, R.S., Berg, E., Williams, C., Clark, T., 2019. Postglacial vegetation community change over an elevational gradient on the western Kenai Peninsula, Alaska: pollen records from Sunken Island and Choquette lakes. *Journal of Quaternary Science* **34**, 309–322.

Anderson, R.S., Hallett, D.J., Berg, E., Jass, R.B., Toney, J.L., de Fontaine, C.S., DeVolder, A., 2006. Holocene development of Boreal forests and fire regimes on the Kenai Lowlands of Alaska. *The Holocene* **16**, 791–803.

Anderson, R.S., Kaufman, D.S., Berg, E., Schiff, C., Daigle, T., 2017. Holocene biogeography of *Tsuga mertensiana* and other conifers in the Kenai Mountains and Prince William Sound, south-central Alaska. *The Holocene* **27**, 485–495.

Appleby, P., 2001. Chronostratigraphic techniques in recent sediments. In: Last, W., Smol., J. (Eds.), *Tracking Environmental Change Using Lake Sediments, vol. 1.* Kluwer Academic Publishers, Dordrecht, The Netherlands, pp. 171–203.

Arp, C.D., Jones, B.M., Grosse, G., 2013. Recent lake ice-out phenology within and among lake districts of Alaska, U.S.A. *Limnology and Oceanography* **58**, 2013–2028.

Ayres, K.R., Sayer, C.D., Skeate, E.R., Perrow, M.R., 2007. Palaeolimnology as a tool to inform shallow lake management: an example from Upton Great Broad, Norfolk, UK. *Biodiversity and Conservation* **17**, 2153–2168.

Bailey, H.L., Kaufman, D.S., Henderson, A.C.G., Leng, M.J., 2015. Synoptic scale controls on the $\delta^{18}O$ in precipitation across Beringia. *Geophysical Research Letters* **42**, 4608–4616.

Bailey, H.L., Kaufman, D.S., Sloane, H.J., Hubbard, A.L., Henderson, A.C.G., Leng, M.J., Meyer, H., Welker, J.M., 2018. Holocene atmospheric circulation in the central North Pacific: A new terrestrial diatom and $\delta^{18}O_{diatom}$ dataset from the Aleutian Islands. *Quaternary Science Reviews* **194**, 27–38.

Bailey, H.L., Klein, E.S., Welker, J.M., 2019. Synoptic and mesoscale mechanisms driver winter precipitation $\delta^{18}O/\delta^{2}H$ in south-central Alaska. *Journal of Geophysical Research: Atmospheres* **124**, 4252–4266.

Barron, J.A., Anderson, L., 2011. Enhanced Late Holocene ENSO/PDO expression along the margins of the eastern North Pacific. *Quaternary International* **235**, 3–12.

Benjamini, Y., Hochberg, Y., 1995. Controlling the false discovery rate: a practical and powerful approach to multiple testing. *Journal of the Royal Statistical Society* **57**, 289–300.

Berg, E.E., Kaufman, D.S., Anderson, R.S., Wiles, G.C., Lowell, T.V., Mitchell, E.A.D, Hu, F.S., Werner, A., in press. Late-glacial and Holocene lake level fluctuations on the Kenai Lowland, reconstructed from satellite-fen peat deposits and ice-shoved ramparts, Kenai Peninsula, Alaska. *Quaternary* **5**.

Berkelhammer, M.B., Stott, L.D., Yoshimura, K., Johnson, K., Sinha, A., 2012. Synoptic and mesoscale controls on the isotopic composition of precipitation in the western United States. *Climate Dynamics* **38**, 433–454.

Bhatia, M.P., Das, S.B., Kujawinski, E.B., Henderson, P., Burke, A., Charette, M.A., 2011. Seasonal evolution of water contributions to discharge from a Greenland outlet glacier: insight from a new isotope-mixing model. *Journal of Glaciology* **57**, 929–941.

Blaauw, M., Christen, J.A., 2011. Flexible paleoclimate age-depth models using an autoregressive gamma process. *Bayesian Analysis* **6**, 457–474.

Bradbury, J.P., Forester, R.M., Thompson, R.S., 1989. Late Quaternary paleolimnology of Walker Lake, Nevada. *Journal of Paleolimnology* **1**, 249–267.

Brandriss, M.E., O'Neil, J.R., Edlund, M.B., Stoermer, E.F., 1998. Oxygen isotope fractionation between diatomaceous silica and water. *Geochimica et Cosmochimica Acta* **62**, 1119–1125.

Bretherton, C.S., Widmann, M., Dymnikov, V.P., Wallace, J.M., Bladé, I., 1999. The effective number of spatial degrees of freedom of a time-varying field. *Journal of Climate* **12**, 1990–2009.

Brewer, T.S., Leng, M.J., Mackay, A.W., Lamb, A.L., Tyler, J.T., Marsh, N.G., 2008. Unraveling contamination signals in biogenic silica oxygen isotope composition: the role of major and trace element geochemistry. *Journal of Quaternary Science* **23**, 321–330.

Broadman, E., Kaufman, D.S., Henderson, A.C.G., Berg. E.E., Anderson, R.S., Leng, M.J., Stahnke, S.A., Muñoz, S.E., 2020. Multi-proxy evidence for millennial-scale changes in North Pacific Holocene hydroclimate from the Kenai Peninsula lowlands, south-central Alaska. *Quaternary Science Reviews* **241**, 106420.

Buczkó, K., Szurdoki, E., Braun, M., Magyari, E., 2018. Reconciling diverse diatom-based lake responses to climate change in four mountain lakes in the South-Carpathian Mountains during the last 17 kyrs. *Quaternary International* **477**, 117–137.

Butz, C., Grosjean, M., Fischer, D., Wunderle, S., Tylmann, W., Rein, B., 2015. Hyperspectral imaging spectroscopy: a promising method for the biogeochemical analysis of lake sediments. *Journal of Applied Remote Sensing* **9**, 096031.

Cayan, D.R., Peterson, D.H., 1989. The influence of North Pacific circulation on streamflow in the West. In: Peterson, D.H. (Ed.), *Aspects of Climate Variability in the Pacific and Western Americas, vol. 55.* American Geophysical Union, Washington, DC, pp. 375–398.

Chapligin, B., Leng, M.J., Webb, E., Alexandre, A., Dodd, J.P., Ijiri, A., Lücke, A., et al., 2011. Inter-laboratory comparison of oxygen isotope compositions from biogenic silica. *Geochimica et Cosmochimica Acta* **75**, 7242–7256.

Clegg, B.F., Kelly, R., Clarke, G.H., Walker, I.R., Hu, F.S., 2011. Nonlinear response of summer temperature to Holocene insolation forcing in Alaska. *Proceedings of the National Academy of Sciences* **108**, 19299–19304.

Cooper, W.S., 1942. Vegetation of the Prince William Sound region, Alaska; with a brief excursion into post-Pleistocene climatic history. *Ecological Monographs* **12**, 1–22.

Craig, H., Gordon, L.I., 1965. Deuterium and oxygen 18 variations in the ocean and marine atmosphere. In: Tongiogi, E. (Ed.), *Stable Isotopes in Oceanographic Studies and Paleotemperatures.* Laboratorio di Geologica Nucleare, Pisa, Italy, pp. 9–130.

Crespin, J., Sylvestre, F., Alexandre, A., Sonzogni, C., Pailles, C., Perga, M-E., 2010. Re-examination of the temperature-dependent relationship between $\delta^{18}O_{diatoms}$ and $\delta^{18}O_{lake water}$ and implications for paleoclimate inferences. *Journal of Paleolimnology* **44**, 547–557.

Crisman, T.L., Crisman, U.A.M., Binford, M.W., 1986. Interpretation of bryozoan microfossils in lacustrine sediment cores. *Hydrobiologia* **143**, 113–118.

Dansgaard, W., 1964. Stable isotopes in precipitation. *Tellus,* **16**, 436–468.

Davies, L.J., Jensen, B.J.L., Froese, D.G., Wallace, K.L., 2016. Late Pleistocene and Holocene tephrostratigraphy of interior Alaska and Yukon: key beds and chronologies over the past 30,000 years. *Quaternary Science Reviews* **146**, 28–53.

Dean, W.E., 1974. Determination of carbonate and organic matter in calcareous sediments and sedimentary rocks by loss on ignition; comparison with other methods. *Journal of Sedimentary Research* **44**, 242–248.

Digerfeldt, G., Almendinger, J.E., Björck, S., 1992. Reconstruction of past lake levels and their relation to groundwater hydrology in the Parkers Prairie sandplain, west-central Minnesota. *Palaeogeography, Palaeoclimatology, Palaeoecology* **94**, 99–118.

Dodd, J.P., Sharp, Z.D., 2010. A laser fluorination method for oxygen isotope analysis of biogenic silica and a new oxygen isotope calibration of modern diatoms in freshwater environments. *Geochimica et Cosmochimica Acta* **74**, 1381–1390.

Dodd, J.P., Sharp, Z.D., Fawcett, P.J., Brearley, A.J., McCubbin, F.M., 2012. Rapid post-mortem maturation of diatom silica oxygen isotope values. *Geochemistry and Geophysics* **13**(9), Q09014.

Dodd, J.P., Wiedenheft, W., Schwartz, J.M., 2017. Dehydroxylation and diagenetic variations in diatom oxygen isotope values. *Geochimica et Cosmochimica Acta* **199**, 185–195.

Du, X., Hendy, I., Hinnov, L., Brown, E., Zhu, J., Poulsen, C.J., 2020. High-resolution interannual precipitation reconstruction of Southern California: implications for Holocene ENSO evolution. *Earth and Planetary Science Letters* **554**, 116670.

Ebisuzaki, W., 1997. A method to estimate the statistical significance of a correlation when the data are serially correlated. *Journal of Climate* **1510**, 2147–2153.

Eilers, J.M., Landers, D.H., Newell, A.D., Mitch, M.E., Morrison, M., Ford, J., 1992. Major ion chemistry of lakes on the Kenai Peninsula, Alaska. *Canadian Journal of Fisheries and Aquatic Sciences* **50**, 816–826.

Faegri, K., Iversen, J., 1989. *Textbook of Pollen Analysis*. John Wiley & Sons, Chichester, United Kingdom.

NSIDC (National Ice Center and National Snow and Ice Data Center), 2018. *Multisensor Analyzed Sea Ice Extent—Northern Hemisphere (MASIE), version 1, Section 16; Cook Inlet.* Compiled by Fetterer, F., Savoie, M., Helfrich, S., and Clemente-Colón. P. 2010, updated daily. Boulder, Colorado USA. https://doi.org/10.7265/N5GT5K3K.

Finkelstein, S.A., Gajewski, K., 2008. Responses of Fragilarioid-dominated diatom assemblages in a small Arctic lake to Holocene climatic changes, Russell Island, Nunavut, Canada. *Journal of Paleolimnology* **40**, 1079–1095.

Fisher, D., Osterberg, E., Dyke, A., Dahl-Jensen, D., Demuth, M., Zdanowicz, C., Bourgeois, J., *et al.*, 2008. The Mt Logan Holocene–late Wisconsinan isotope record: tropical Pacific–Yukon connections. *The Holocene* **18**, 667–677.

Foged N., 1971. Diatoms found in a bottom sediment sample from a small deep lake on the Northern Slope, Alaska. *Nova Hedwigia* **21**: 923–1034.

Foged, N., 1981. Diatoms in Alaska. *Bibliotheca Phycologica* **53**, 1–317.

Francis, D.R., 2001. Bryozoan statoblasts. In: Smol, J.P., Birks, H.J.B., Last, W.M. (Eds.), *Tracking Environmental Change Using Lake Sediments, vol. 4: Zoological Indicators.* Springer, New York, pp. 105–124.

Gibson, J.J., Prepas, E.E., McEachern, P., 2002. Quantitative comparison of lake throughflow, residency, and catchment runoff using stable isotopes: modeling and results from a regional survey of Boreal lakes. *Journal of Hydrology* **262**, 128–144.

Gonfiantini, R., 1986. Environmental isotopes in lake studies. In: Fritz, P., Fontes, J. (Eds.), *Handbook of Environmental Isotope Geochemistry, vol 3.* Elsevier, New York, pp. 113–168.

Grimm, E.C., 1987. CONISS—a Fortran-77 program for stratigraphically constrained cluster-analysis by the method of incremental sum of squares. *Computational Geoscience* **13**, 13–35.

Grimm, E.C., Maher, L.J., Jr., Nelson, D.M., 2009. The magnitude of error in conventional bulk-sediment radiocarbon dates from central North America. *Quaternary Research* **72**, 301–308.

Hartikainen, H., Johnes, P., Moncrieff, C., Okamura, B., 2009. Bryozoan populations reflect nutrient enrichment and productivity gradients in rivers. *Freshwater Biology* **54**, 2320–2334.

Hayward, G.D., Colt, S., McTeague, M.L., Hollingsworth, T.N., 2017. Climate change vulnerability assessment for the Chugach National Forest and the Kenai Peninsula. *General Technical Report PNW-GTR-950.* U.S. Department of Agriculture, Forest Service, Pacific Northwest Research Station, Portland, Oregon, 340 pp.

Henne, P.D., Elkin, C.M., Reineking, B., Bugmann, H., Tinner, W., 2011. Did soil development limit spruce (*Picea abies*) expansion in the Central Alps during the Holocene? Testing a palaeobotanical hypothesis with a dynamic landscape model. *Journal of Biogeography* **38**, 933–949.

Horita, J., Wesolowski, D.J., 1994. Liquid-vapor fractionation of oxygen and hydrogen isotopes of water from the freezing to the critical temperature. *Geochimica et Cosmochimica Acta* **58**, 3425–3437.

Hosono, T., Yamada, C., Manga, M., Wang, C.-Y., Tanimizu, M., 2020. Stable isotopes show that earthquakes enhance permeability and release water from mountains. *Nature Communications* **11**, 2776.

Hu, F.S., Finney, B.P., Brubaker, L.B., 2001. Effects of Holocene *Alnus* expansion on aquatic productivity, nitrogen cycling, and soil development in southwestern Alaska. *Ecosystems* **4**, 358–368.

Ide, K., Hosono, T., Kagabu, M., Fukamizu, K., Tokunaga, T., Shimada, J., 2020. Changes of groundwater flow systems after the 2016 M_W 7.0 Kumamoto earthquake deduced by stable isotopic and CFC-12 compositions of natural springs. *Journal of Hydrology* **583**, 124551.

Jackson, S.T., Booth, R.K., Reeves, K., Anderson, J.J., Minckley, T.A., Jones, R.A., 2014. Inferring local to regional changes in forest composition from Holocene macrofossils and pollen of a small lake in central upper Michigan. *Quaternary Science Reviews* **98**, 60–73.

Jones, M.C., Anderson, L., Keller, K., Nash, B., Littell, V., Wooller, M., Jolley, C.A., 2019. An assessment of plant species differences on cellulose oxygen isotopes from two Kenai Peninsula Alaska peatlands: implications for hydroclimatic reconstructions. *Frontiers in Earth Science* **7**, 1–25.

Jones, M.C., Wooller, M., Peteet, D.M., 2014. A deglacial and Holocene record of climate variability in south-central Alaska from stable oxygen isotopes and plant macrofossils in peat. *Quaternary Science Reviews* **87**, 1–11.

Juggins, S., 2017. *Rioja: Analysis of Quaternary Science Data, R package*, version (0.9-21). http://cran.r172project.org/package=rioja.

Juillet-Leclerc, A., Labeyrie, L., 1987. Temperature dependence of the oxygen isotopic fractionation between diatom silica and water. *Earth and Planetary Science Letters* **84**, 69–74.

Kalnay, E., Manamitsu, M., Kistler, R., Collins, W., Deaven, D., Gandin, L., Iredell, M., *et al.*, 1996. The NCEP/NCAR 40-year reanalysis project. *Bulletin of the American Meteorological Society* **77**, 437–470.

Karlstrom, T.N.V., 1964. Quaternary geology of the Kenai Lowland and glacial history of the Cook Inlet region, Alaska. *U.S. Geological Survey Professional Paper* **443**. https://doi.org/10.3133/pp443.

Kaufman, D.S., Anderson, R.S., Hu, F.S., Berg, E., Werner, A., 2010. Evidence for a variable and wet Younger Dryas in southern Alaska. *Quaternary Science Reviews* **29**, 1445–1452.

Kaufman, D.S., Axford, Y., Anderson, R.S., Lamoureux, S.F., Schindler, D.E., Walker, I.R., Werner, A., 2012. A multi-proxy record of the Last Glacial Maximum and last 14,500 years of paleoenvironmental change at Lone Spruce Pond, southwestern Alaska. *Journal of Paleolimnology* **48**, 9–26.

Kaufman, D.S., Axford, Y.L., Henderson, A.C.G., McKay, N.P., Oswald, W.W., Saenger, C., Anderson, R.S., *et al.*, 2016. Holocene climate changes in eastern Beringia (NW North America)—a systematic review of multi-proxy evidence. *Quaternary Science Reviews* **147**, 312–339.

Koning, E., Gehlen, M., Flank, A.M., Calas, G., Epping, E., 2007. Rapid post-mortem incorporation of aluminum in diatom frustules: evidence from chemical and structural analyses. *Marine Chemistry* **106**, 208–222.

Kopczynski, S.E., Kelley, S.E., Lowell, T.V., Evenson, E.B., Applegate, P.J., 2017. Latest Pleistocene advance and collapse of the Matanuska-Knik glacier system, Anchorage Lowland, southern Alaska. *Quaternary Science Reviews* **156**, 121–134.

Krabbenhoft, D.P., Bowser, C.J., Anderson, M.P., Valley, J.W., 1990. Estimating Groundwater Exchange with Lakes: 1. The Stable Isotope Mass Balance Method. *Water Resources Research* **26**(10), 2445–2453.

Krammer, K., Lange-Bertalot, H., 1986–1991. *Bacillariophyceae Band 1–4.* Gustav Fischer Verlag, Stuttgart, Germany.

Krawiec, A.C.L., Kaufman, D.S., 2014. Holocene storminess inferred from sediments of two lakes on Adak Island, Alaska. *Quaternary Research* **82**, 73–84.

Lacey, J.H., Jones, M.D., 2018. Quantitative reconstruction of Early Holocene and last glacial climate on the Balkan Peninsula using coupled hydrological and isotope mass balance modeling. *Quaternary Science Reviews* **202**, 109–121.

Landhausser, S.M., Silins, U., Lieffers, V.J., Liu, W., 2003. Response of *Populus tremuloides*, *Populus balsamifera*, *Betula papyrifera* and *Picea glauca* seedlings to low soil temperature and water-logged soil conditions. *Scandinavian Journal of Forest Research* **18**, 391–400.

Leng, M.J., Barker, P.A., 2006. A review of the oxygen isotope composition of lacustrine diatom silica for palaeoclimate reconstruction. *Earth-Science Reviews* **75**, 5–27.

Leng, M.J., Sloane, H.J., 2008. Combined oxygen and silicon isotope analysis of biogenic silica. *Journal of Quaternary Science* **23**, 313–319.

Liljedahl, A.K., Gädeke, A., O'Neel, S., Gatesman, T.A., Douglas, T.A., 2017. Glacierized headwater streams as aquifer recharge corridors, subarctic Alaska. *Geophysical Research Letters* **44**, 6876–6885.

Linacre, E., 1992. *Climate Data and Resources: a Reference and Guide.* Routledge, London.

Lotter, A.F., Hofmann, G., 2003. The development of the late-glacial and Holocene diatom flora in Lake Sedmo Rilsko (Rila Mountains, Bulgaria). In: Tonkov, S. (Ed.), *Aspects of Palynology and Palaeoecology.* Pensoft Publishers, Moscow, pp. 171–183.

Mann, D.G., McDonald, S.M., Mayer, M.M., Droop, S.J.M., Chepurnov, V.A., Loke, R.E., Ciobanu, A., Du Buf, J.M.H., 2004. The *Sellaphora pupula* species complex (Bacillariophyceae): morphometric analysis, ultrastructure and mating data provide evidence for five new species. *Phycologia* **43**, 459–482.

McKay, N.P., Emile-Geay, J., Khinder, D., 2021. GeoChronR—an R package to model, analyze and visualize age-uncertain paleoscientific data. *Geochronology* **3**, 149–169.

McKay, N.P., Kaufman, D.S., 2009. Holocene climate and glacier variability at Hallet and Greyling lakes, Chugach Mountains, south-central Alaska. *Journal of Paleolimnology* **41**, 143–159.

McKay, N.P., Kaufman, D.S., Michelutti, N., 2008. Biogenic silica concentration as a high resolution, quantitative temperature proxy at Hallet Lake, south-central Alaska. *Geophysical Research Letters* **35**, L05709.

McLaughlin, R.B., Stone, J.L., 1986. Some Late Pleistocene diatoms of the Kenai Peninsula, Alaska. *Nova Hedwigia* **82**, 1–148.

Menicucci, A.J., Spero, H.J., Matthews, J., Parikh, S.J., 2017. Influence of exchangeable oxygen on biogenic silica oxygen isotope data. *Chemical Geology* **466**, 710–721.

Messender, A.S., 1980. Spruce plantation effects on soil moisture and chemical element distribution. *Forest Ecology and Management* **3**, 113–125.

Mock, C.J., Bartlein, P.J., Anderson, P.M., 1998. Atmospheric circulation patterns and spatial climatic variations in Beringia. *International Journal of Climatology* **10**, 1085–1104.

Morley, D.W., Leng, M.J., Mackay, A.W., Sloane, H J., Rioual, P., Battarbee, R.W., 2004. Cleaning of lake sediment samples for diatom oxygen isotope analysis. *Journal of Paleolimnology* **31**, 391–401.

Mortlock, R.A., Froelich, P.N., 1989. A simple method for the rapid determination of biogenic opal in pelagic marine sediments. *Deep-Sea Research* **36**, 1415–1426.

Moschen, R., Lücke, A., Schleser, G.H., 2005. Sensitivity of biogenic silica oxygen isotopes to changes in surface water temperature and paleoclimatology. *Geophysical Research Letters* **32**, L07708.

Nesje, A., Dahl, S.O., 2001. The Greenland 8200 cal. yr BP event detected in loss-on-ignition profiles in Norwegian lacustrine sediment sequences. *Journal of Quaternary Science* **16**, 155–166.

Oksanen, J., Kindt, R., Legendre, P., O'Hara, B., Henry, M., Stevens, H., 2007. The vegan package. *Community Ecology Package* **10**, 631–637.

Orlova, M.A., Lukina, N.V., Smirnov, V.E., Artemkina, N.A., 2016. The influence of spruce on acidity and nutrient content in soils of northern Taiga dwarf shrub-green moss spruce forests. *Eurasian Soil Science* **49**, 1276–1287.

Overland, J.E., Adams, J.M., Bond, N.A., 1999. Decadal variability of the Aleutian Low and its relation to high-latitude circulation. *Journal of Climate* **12**, 1542–1548.

Paillard, D., Labeyrie, L., Yiou, P., 1996. Macintosh program performs time-series analysis. *Eos* **77**, 379.

Penman, H.L., 1948. Natural evaporation from open water, bare soil and grass. *Proceedings of the Royal Society A—Mathematical, Physical, and Engineering Sciences* **193**, 120–145.

Perren, B.B., Axford, Y., Kaufman, D.S., 2017. Alder, nitrogen, and lake ecology: terrestrial-aquatic linkages in the postglacial history of Lone Spruce Pond, southwestern Alaska. *PLoS ONE* **12**(1), e0169106.

Philippsen, B., 2013. The freshwater reservoir effect in radiocarbon dating. *Heritage Science* **1**, 24.

Porter, T.J., Pisaric, M.F.J., Field, R.D., Kokelj, T.W.D., deMontigny, P., Healy, R., LeGrande, A.N., 2014. Spring-summer temperatures since AD 1780 reconstructed from stable oxygen isotope ratios in white spruce tree-rings from the Mackenzie Delta, northwestern Canada. *Climate Dynamics* **42**, 771–785.

Pukacz, A., Pełechaty M., Frankowski, M., 2016. Depth-dependence and monthly variability of charophyte biomass production: consequences for the precipitation of calcium carbonate in a shallow *Chara*-lake. *Environmental Science and Pollution Research* **23**, 22433–22442.

Ranger, J., Nys, C., 1994. The effect of spruce (*Picea abies* Karst.) on soil development: an analytical and experimental approach. *European Journal of Soil Science* **45**, 193–204.

Reger, R.D., Combellick, R.A., Brigham-Grette, J., 1995. Update of latest Wisconsin events in the upper Cook Inlet region, southcentral Alaska. In: Combellick, R.A., Tannian, F. (Eds.), *Short Notes on Alaska Geology 1995.* Alaska Division of Geological & Geophysical Surveys Professional Report **111**, p. 45–53.

Reger, R.D., Lowell, T., Evenson, E.B., 2011. Discussion of "Late Quaternary megafloods from Glacial Lake Atna, Southcentral Alaska, U.S.A." *Quaternary Research* **75**, 301–302.

Reger, R.D., Sturmann, A.G., Berg, E.E., Burns, P.A.C., 2007. *A Guide to the Late Quaternary History of Northern and Western Kenai Peninsula, Alaska: Guidebook 8.* State of Alaska Department of Natural Resources, Division of Geological and Geophysical Surveys, Anchorage, Alaska.

Reger, R.D., Updike, R.G., 1983. Upper Cook Inlet region and the Matanuska Valley. In: Péwé, T.L., Reger, R.D. (Eds.), *Guidebook to Permafrost and Quaternary Geology Along the Richardson and Glenn Highways Between Fairbanks and Anchorage, Alaska.* Alaska Division of Geological & Geophysical Surveys Guidebook **1**, p. 185–263, 1 sheet, scale 1:250,000.

Reimer, P., Austin, W.E.N., Bard, E., Bayliss A., Blackwell P.G., Bronk Ramsey C., Butzin M., *et al.*, 2020. The IntCal20 Northern Hemisphere radiocarbon age calibration curve (0–55 cal kBP). *Radiocarbon* **62**, 725–757.

Rein, B., Sirocko, F., 2002. In-situ reflectance spectroscopy-analyzing techniques for high resolution pigment logging in sediment cores. *International Journal of Earth Science* **91**, 950–954.

Rodionov, S.N., Bond, N.A., Overland, J.E., 2007. The Aleutian Low, storm tracks, and winter climate variability. *Deep-Sea Research II* **54**, 2560–2577.

Santos, G.M., Moore, R.B., Southon, J.R., Griffin, S., Hinger, E., Zhang, D., 2007. AMS ^{14}C sample preparation at the KCCAMS/UCI facility: status report and performance of small samples. *Radiocarbon* **49**, 255–269.

Schiff, C., Kaufman, D.S., Wolfe, A.P., Dodd, J., Sharp, Z., 2009. Late Holocene storm-trajectory changes inferred from the oxygen isotope composition of lake diatoms, south Alaska. *Journal of Paleolimnology* **41**, 189–208.

Shaftel, R.S., King, R.S., Back, J.A., 2011. Alder cover drives nitrogen availability in Kenai lowland headwater streams, Alaska. *Biogeochemistry* **107**, 135–148.

Shemesh, A., Charles, C.D., Fairbanks, R.G., 1992. Oxygen isotopes in biogenic silica: global changes in ocean temperature and isotopic composition. *Science* **256**, 1434–1436.

Shuman, B., 2003. Controls on loss-on-ignition variation in cores from two shallow lakes in the northeastern United States. *Journal of Paleolimnology* **30**, 371–385.

Singarayer, J.S., Valdes, P.J., 2010. High-latitude climate sensitivity to ice-sheet forcing over the last 120 kyr. *Quaternary Science Reviews* **29**, 43–55.

Šmejkalová, T., Edwards, M., Dash, J., 2016. Arctic lakes show strong decadal trend in earlier spring ice-out. *Scientific Reports* **6**, 38449.

Spaulding, S.A., Bishop, I.W., Edlund, M.B., Lee, S., Potapova, M., 2020. *Diatoms of North America.* https://diatoms.org/. [accessed 24 Dec 2020]

Steinman, B.A., Rosenmeier, M.F., Abbott, M.B., Bain, D.J., 2010. The isotopic and hydrologic response of small, closed-basin lakes to climate forcing from predictive models: application to paleoclimate studies in the upper Columbia River basin. *Limnology and Oceanography* **55**, 2231–2245.

ter Braak, C.J.F., Prentice, I.C., 1988. A theory of gradient analysis. *Advances in Ecological Research* **18**, 271e317.

Tyler, J.J., Sloane, H.J., Rickaby, R.E.M., Cox, E.J., Leng, M.J., 2017. Post-mortem oxygen isotope exchange within cultured diatom silica. *Rapid Communications in Mass Spectrometry* **31**, 1749–1760.

Valentino, J.D., Owen, L.A., Spotila, J.A., Cesta, J.M., Caffee, M.W., 2021. Timing and extent of Late Pleistocene glaciation in the Chugach Mountains, Alaska. *Quaternary Research* **101**, 205–224.

Vallentyne, J.R., 1957. Principles of modern limnology. *American Scientist* **45**, 218–244.

Van den Berg, M.S., Coops, H., Simons, J., 2001. Propagule bank buildup of *Chara aspera* and its significance for colonization of a shallow lake. *Hydrobiologia* **462**, 9–17.

Ventura, V., Paciorek, C.J., Risbey, J.S., 2004. Controlling the proportion of falsely rejected hypotheses when conducting multiple tests with climatological data. *Journal of Climate* **17**, 4343–4356.

Wallace, K.L., Coombs, M.L., Hayden, L.A., Waythomas, C.F., 2014. Significance of a near-source tephra-stratigraphic sequence to the eruptive history of Hayes volcano, south-central Alaska. *US Geological Survey Scientific Investigations Report* 2014-5133, 32 pp. https://doi.org/10.3133/sir20145133.

Wang, L., Mackay, A.W., Leng, M.J., Rioual, P., Panizzo, V.N., Lu, H., Gu, Z., Chu, G., Han, J., Kendrick, C.P., 2013. Influence of the ratio of planktonic to benthic diatoms on lacustrine organic matter $\delta^{13}C$ from Erlongwan maar lake, northeast China. *Organic Geochemistry* **54**, 62–68.

Wiedmer, M., Montgomery, D.R., Gillespie, A.R., Greenberg, H., 2010. Late Quaternary megafloods from Glacial Lake Atna, southcentral Alaska, U.S.A. *Quaternary Science Reviews* **73**, 413–424.

Wolfe, A.P., Vinebrooke, R.D., Michelutti, N., Rivard, B., Das, B., 2006. Experimental calibration of lake-sediment spectral reflectance to chlorophyll-*a* concentrations: methodology and paleolimnological validation. *Journal of Paleolimnology* **36**, 91–100.

Wolin, J.A., Duthie, H.C., 1999. Diatoms as indicators of water level change in freshwater lakes. In: Smol, J.P., Stoermer, E.F. (Eds.), *The Diatoms: Application for the Environmental and Earth Sciences.* Cambridge University Press, Cambridge, United Kingdom, pp. 183–202.

Wood, T.S., 2001. Bryozoans. In: Thorp, J.H., Covich, A.P. (Eds.), *Ecology and Classification of North American Freshwater Invertebrates, 2nd Edition.* Elsevier, Amsterdam, The Netherlands, pp. 505–525.

Wrobleski, E.A., 2021. *Multi-Proxy Evidence for Climatic and Environmental Change During the Late Glacial and Holocene at Kelly Lake, Kenai Peninsula, Alaska.* Master's thesis, Northern Arizona University, Flagstaff, Arizona. ProQuest ID 28714852, https://openknowledge.nau.edu/id/eprint/5706/

Yu, Z., Walker, K.N., Evenson, E.B., Hajdas, I., 2008. Lateglacial and Early Holocene climate oscillations in Matanuska Valley, south-central Alaska. *Quaternary Science Reviews* **27**, 148–161.

Zhao, Y., Sayer, C.D., Birks, H.H., Hughes, M., Peglar, S.M., 2006. Spatial representation of aquatic vegetation by macrofossils and pollen in a small and shallow lake. *Journal of Paleolimnology* **35**, 335–350.